Heliyon 10 (2024) e26320

Contents lists available at ScienceDirect

Heliyon

journal homepage: www.cell.com/heliyon

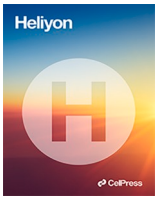

Research article

A generalized analytical energy balance model for evaluating agglomeration from a binary collision of wet particles

Jaber Shabanian [a,b,*], Marc A. Duchesne [a], Madhava Syamlal [c], Allan Runstedtler [a]

[a] Natural Resources Canada, CanmetENERGY, 1 Haanel Drive, Ottawa, Ontario K1A 1M1, Canada
[b] Process Engineering Advanced Research Lab, Department of Chemical Engineering, Polytechnique Montreal, C.P. 6079, succ. Centre-Ville, Montreal, Quebec H3C 3A7, Canada
[c] National Energy Technology Laboratory, U.S. Department of Energy, Morgantown, WV 26507-0880, United States

ARTICLE INFO

Keywords:
Wet particle agglomeration
Liquid bridge
Analytical energy balance model
Granulation
Gas-solid fluidized bed
Thermal conversion

ABSTRACT

Agglomeration of wet particles, i.e., particles coated with a thin liquid layer, is a common phenomenon in many processes like fluidized bed combustion of low rank fuels. The availability of an agglomeration model that can evaluate the outcome of a binary collision between wet particles differing in solid particle properties, liquid layer thicknesses, and initial collision (impact) speeds is essential for obtaining a comprehensive understanding on the existing processes experiencing wet particle agglomeration or for a successful development of new processes with high chances of wet particle agglomeration. This study presents a generalized agglomeration model on the basis of energy conservation before and after collision when colliding wet particles may differ in solid particle properties, liquid layer thicknesses, and impact speeds. The model was established based on the approximate values of energy losses that may happen during the collision. It incorporates body forces, solid-solid contacting, liquid capillary, and viscous contributions, as well as the liquid bridge volume effect. Predictions of the new model for collision outcomes of identical wet particles were like those from an analytical energy balance model developed recently by the group for identical wet particles. We also validated the new model by experimental data from literature. The results of a collision direction analysis indicated that the direction often has a minimal effect on the collision outcome in many practical scenarios. The results of Monte Carlo uncertainty analyses with the new model revealed that proper estimations of impact speed, under capillary limiting conditions, and thickness of coating layers and asperity heights, under viscous limiting conditions, are critical for the realistic prediction of collision outcomes at impact speeds close to critical impact speed, i.e., the minimum particle speed required for the particles to rebound.

1. Introduction

Wet granulation, drying, food processing, pharmaceutical manufacturing, and combustion and gasification of fuels in high temperature gas-solid fluidized bed reactors are among processes that commonly experience wet particle agglomeration [1–4]. A small amount of liquid that is injected or produced throughout these processes may coat the particles and, hence, can serve as an agent for binding particles [4,5], i.e., their agglomeration. Wet particle agglomerates form owing to an increase in the level of liquid

* Corresponding author. Natural Resources Canada, CanmetENERGY, 1 Haanel Drive, Ottawa, Ontario K1A 1M1, Canada.
E-mail addresses: jaber.shabanian@polymtl.ca, jaber.shabanian@nrcan-rncan.gc.ca (J. Shabanian).

https://doi.org/10.1016/j.heliyon.2024.e26320
Received 3 February 2024; Accepted 9 February 2024
Available online 13 February 2024

bridge-induced cohesive interparticle forces that dominate repulsive forces. Depending on when and where it occurs, particle agglomeration may be beneficial or deleterious [6]. In certain circumstances, e.g., thermal conversion of fuels (gasification/combustion of low-quality solid fuels and addition of alkali materials to combustors for air pollution control) in high temperature gas-solid fluidized bed reactors, the formation and continuous growth of agglomerates are undesirable as they can yield a complete blockage of distributor plates and/or bed defluidization and, hence, forced plant shutdowns [7,8]. Downtime, production loss, a cumbersome cleaning step, and restarting of the plant will accordingly be resulted. Since these macroscopic outcomes are yielded from microscopic phenomena occurring on the surface of bed particles and the corresponding interactions between particles, a thorough description of the collision behavior of two particles is an essential building block for an intimate understanding of particle agglomeration.

Extensive studies on the outcome of a collision between wet solid surfaces, principally a binary collision of identical wet particles or a wet collision between a particle and a plate, (agglomeration or rebound) are reported in literature through either experiment [9–13] or modeling. One can classify the latter category in three groups on the basis of adopted assumptions: (i) some assumed that collision behavior is dominated by capillary effects [6,14–17]; (ii) some postulated that viscous effects are dominant [18–26]; and (iii) others considered that both the capillary and viscous effects simultaneously govern the collision behavior [2,27–32]. The proposed models in most of these studies, except the one proposed by Balakin et al. [29], are for a binary collision of identical wet particles or a wet collision between a particle and a plate. A particle assembly can, however, be made of particles differing in solid particle properties (including the size, material, and asperity characteristics) and initial collision speeds. In addition, in the case of particles having a highly wetting liquid coating, i.e., with a contact angle approaching zero degrees, it is possible that the coating is non-uniformly distributed among the base particles leading to wet particles of different coating thicknesses in the system. An oxygen carrier assisted combustion process [33,34] is a good example where all these dissimilarities between wet particles can be experienced. Through this process, a bed may be made of particles with, e.g., ilmenite ore, and without, e.g., silica sand, oxygen carrying properties. The two bed materials typically have different particle size distributions, to show similar hydrodynamic characteristics in the bed, and asperity sizes. As these particles interact differently with liquid forming substances, e.g., alkali materials from fuel ash, different amounts of liquids may form on the surfaces of these base particles leading to different liquid thicknesses. In addition, due to the heterogeneous gas-solid flow structure in a gas-solid fluidized bed, a range of initial collision speeds can be experienced for each bed material. Although Balakin et al. [29] focused on a binary collision of non-identical wet particles, they did not take the liquid bridge volume effect into account in the calculations, which is a critical consideration when the liquid bridge volume is small [35,36].

The current study presents a generalized analytical energy balance model that simultaneously considers the effects of body forces, solid-solid contacting, and liquid bridge volume-corrected capillary and viscous forces in predicting the outcome of a binary wet particle collision. In addition, it accounts for the collision of wet particles with different liquid layer thicknesses, asperity heights, and initial collision speeds (Section 2). Comparison between the predictions of the generalized agglomeration model with those from an analytical energy balance model for identical wet particles developed recently by the group [31] was also completed (Section 3.1). We validated the generalized agglomeration model by experimental data from literature (Section 3.2). We further investigated the effects of collision direction together with some particle and liquid properties on collision outcome (Section 3.3). Lastly, Monte Carlo uncertainty analyses were conducted to highlight the importance of proper estimations of the model's input parameters (Section 3.4).

2. Model development

2.1. Problem description and assumptions

A two-dimensional schematic representation of a binary collision involving non-identical wet particles is shown in Fig. 1. In this diagram, the speeds of the target particle i, u_i, and colliding neighbor particle j, u_j, are based on the laboratory reference frame I. $u_{0,i}$ and $u_{0,j}$ are respectively the initial (impact) speeds of particles i and j with respect to the reference frame I, $d_{p,s,i}$ is the diameter of solid particle i, and $r_{p,s,j}$ is the radius of solid particle j. $h_{0,i}$ and $h_{0,j}$ are the thickness of coating layers on the surfaces of particles i and j, $h_{a,i}$ and $h_{a,j}$ are the height of asperities on the surfaces of particles i and j, and $\vec{n}_{ij}$ and $\vec{n}_{ji}$ are respectively the unit vectors normal to the surfaces of particles i and j along the axis of collision. d is the separation distance between the centers of the colliding particles and D is the minimum separation distance between the surfaces (excluding asperities) of these particles. $\vec{n}_{ij}$ and $\vec{n}_{ji}$ can be expressed by the following [37]:

$$\vec{n}_{ij} = \frac{\vec{x}_j - \vec{x}_i}{\left|\vec{x}_j - \vec{x}_i\right|} \tag{1}$$

$$\vec{n}_{ji} = \frac{\vec{x}_i - \vec{x}_j}{\left|\vec{x}_i - \vec{x}_j\right|} \tag{2}$$

where $\vec{x}_i$ and $\vec{x}_j$ are the center position vectors of particles i and j. To simplify the calculations of liquid bridge-induced interparticle forces acting on the colliding wet particles and corresponding energy losses, the Derjaguin approximation [38,39] was employed in this study to convert a system of unequally sized particles into a system of identically sized particles with similar magnitudes of

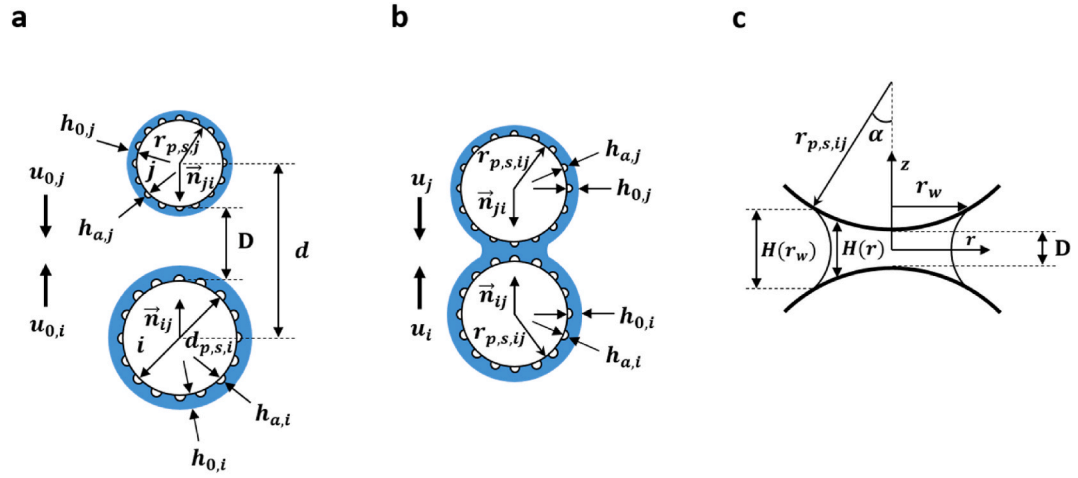

Fig. 1. Schematic representation of a) two approaching non-identical wet particles, b) their Derjaguin approximation, and c) the formation of the liquid bridge between them.

corresponding interparticle forces. According to the Derjaguin approximation, the magnitude of a short range interparticle force between particles of unequal size can be estimated by the expression of the same interparticle force between two identically sized particles and substituting the particle radius with the harmonic mean particle radius when D is much smaller than the radii of the particles [38,39]. Hence, $r_{p,s,ij}$ in Fig. 1 represents the harmonic mean solid particle radius, which is given by:

$$r_{p,s,ij} = \frac{2\, r_{p,s,i}\, r_{p,s,j}}{r_{p,s,i} + r_{p,s,j}} \tag{3}$$

where $r_{p,s,i}$ is the radius of solid particle i. Moreover, in Fig. 1, α is the half-filling angle, r_w is the wetting radius (at $D = h_{a,i} + h_{a,j}$), and $H(r)$ is the separation distance between two colliding wet particles for $0 \le r \le r_w$, where r is the radial distance relative to the bridge center. It is worth noting that owing to geometric limitations, $r_w \le r_{p,s,ij}$. Assuming a cylindrical liquid bridge between the colliding particles, following Pitois et al. [40] and Darabi et al. [2], $H(r)$ can be calculated as follows:

$$H(r) = D + \frac{r^2}{r_{p,s,ij}} \tag{4}$$

The general assumptions made in this study to develop a theoretical background for evaluating the outcome of a binary collision between wet particles are reported in the following list.

i) Colliding solid particles are spherical.
ii) Total mass of a particle is minimally affected by asperities.
iii) Particles are uniformly coated with a liquid layer. Readers are referred to work by Lubarda and Talke [41] for the procedure to estimate the spreading area of a liquid droplet on a surface.
iv) The liquid bridge has uniform physical properties.
v) The difference in the contact angle, θ, for solid particles of dissimilar materials has a negligible contribution to the collision outcome in a highly wetting system [31]. Hence, an average value of θ will be employed in the calculations.
vi) The liquid bridge connecting the particles forms instantaneously, i.e., we disregard partial gas-film drainage effects that may impede the coalescence of liquid coatings. Interested readers are referred to Shabanian et al. [31] for further details.
vii) The liquid bridge volume remains unchanged during the collision interval.
viii) The half-filling angle experiences no change with separation distance.
ix) The height of liquid at the wetting radius, upon initial liquid contact, is the summation of the thickness of liquid layers from the colliding particles, i.e., $H(r_w) = h_{0,i} + h_{0,j}$.
x) The tangential component of the viscous force is negligible.
xi) Particles hydrodynamically interact with the same fluid.
xii) The magnitudes of body forces, i.e., buoyant, drag, and gravity, remain constant and equal to their corresponding values at the time of liquid coating-liquid coating impact, also referred to as the impact condition here, during the collision interval.
xiii) The unit vectors $\vec{n}_{ij}$ and $\vec{n}_{ji}$ calculated at the impact condition remain unchanged during the collision interval.
xiv) The velocity of the center of mass of the colliding particles with respect to the frame I along $\vec{n}_{ij}$, $\vec{u}_{CM,\vec{n}_{ij}}$, remains constant and equal to its value at the impact condition $\vec{u}_{0,CM,\vec{n}_{ij}}$ during the approach stage.

xv) The slight change in $\overrightarrow{u}_{CM,\overrightarrow{n}_{ij}}$ that may happen due to the net effect of body (external) forces on the colliding particles during the approach stage is applied at the end of the approach stage.
xvi) The solid-solid contact happens instantaneously.
xvii) $\overrightarrow{u}_{CM,\overrightarrow{n}_{ij}}$ remains constant and equal to its value at the beginning of the separation stage during the separation stage.
xviii) Binary collision between wet particles is an adiabatic process.

Assumptions (iv) and (ix) allow the generalized model to work for a dry particle impacting a wet particle. Assumption (vi) allows to consider the liquid bridge behaves similarly during the approach and separation stages [2]. If colliding wet particles rebound from each other, they have to pass through three stages: approach, solid-solid contact, and separation. Considering assumption (vi), in the approach stage, the minimum separation distance between particles (D) decreases from $h_{0,i} + h_{0,j}$ to $h_{a,i} + h_{a,j}$. In a highly wetting system, each colliding particle gains energy owing to the liquid bridge capillary effect during the approach stage, while it loses energy due to the liquid bridge viscous effect. The net of body forces acting on the target particle i along $\overrightarrow{n}_{ij}$ acts in the opposite direction of the similar net of forces on the neighbor particle j along $\overrightarrow{n}_{ji}$, while their magnitudes could be identical/different (see Fig. 4 for details). Hence, the kinetic energy of each colliding particle may increase, decrease or remain unvaried due to the net effect of body forces during the approach stage. The solid-solid contact stage starts from the end of the approach stage ($D = h_{a,i} + h_{a,j}$) and the particles make either an elastic or inelastic solid-solid collision with a dry restitution coefficient e. The kinetic energy of each colliding particle remains unchanged for elastic dry-dry particle collision, i.e., $e = 1$, and decreases owing to an inelastic solid-solid contact with $0 \leq e < 1$. In the separation stage, D may increase from $h_{a,i} + h_{a,j}$ to a minimum separation distance between two colliding wet particles at the point of liquid bridge rupture h_{rupt}. The kinetic energy of each colliding particle decreases in the separation stage due either to the liquid bridge capillary or viscous effect. However, similar to the approach stage, it may increase, decrease or remain unchanged due to the net effect of body forces during the separation stage. The colliding wet particles may agglomerate during either the approach or separation stage if the total energy dissipation by them is greater than the relative initial kinetic energy of the particles.

Operating conditions, including the system temperature and pressure, superficial gas velocity, and introduction of specific materials to the system, can change the gas properties, type of liquid formed and its extent in the system, type and extent of sintering propensity of particles, and relative velocities between particles and flowing gas and those between colliding particles. These, subsequently, alter hydrodynamic, interparticle, and collision forces acting on particles in a gas-solid fluidized bed, thus the collision outcomes of (cohesive) particles in the bed. Interested readers are encouraged to refer to Shabanian and Chaouki [42] for detailed discussions on this matter. When employing unconventional heating approaches, e.g., microwave heating, in a gas-solid system, an appreciable temperature difference could be experienced between the gas and solid phases [43–45]. Hence, relevant gas and solid temperatures need to be considered for tracking the magnitudes of hydrodynamic, interparticle, and collision forces acting on the colliding particles.

2.2. Equation of motion and frame of reference

The general equation of motion of a target particle i during a sole binary wet collision with a colliding neighbor particle j can be described by Newton's second law of motion as follows:

$$m_{p,i}\frac{d\overrightarrow{u}_i}{dt} = \overrightarrow{F}_{cont,ij} + \overrightarrow{F}_{drag,i} + \overrightarrow{F}_{buoy,i} + \overrightarrow{W}_i + \overrightarrow{F}_{vis,i} + \overrightarrow{F}_{cap,i} \tag{5}$$

where $m_{p,i}$ is the mass of the target wet particle i, $\overrightarrow{u}_i$ is the velocity of particle i with respect to the reference frame I, and t is time. $\overrightarrow{F}_{cont,ij}$, $\overrightarrow{F}_{drag,i}$, $\overrightarrow{F}_{buoy,i}$, $\overrightarrow{F}_{vis,i}$ and $\overrightarrow{F}_{cap,i}$ are the vector of the solid-solid contact force between the colliding particles i and j, drag force, buoyant force, viscous force, and capillary force acting on particle i, respectively. $\overrightarrow{W}_i$ is the weight vector of particle i. The general equations of motion of the target particle i and the colliding neighbor particle j form the basis for development of a generalized

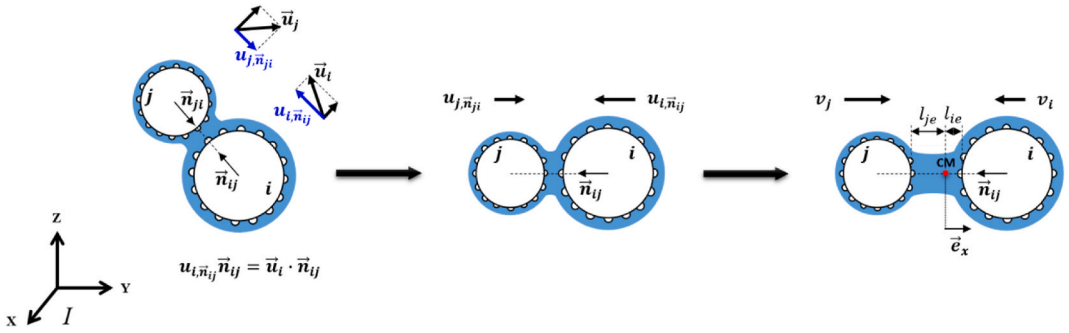

Fig. 2. Conversion of colliding particle velocities from the laboratory reference frame I into a frame with respect to the center of mass of the colliding particles along the normal collision axis.

analytical energy balance model for evaluating agglomeration from a binary collision involving wet particles.

To evaluate the outcome of a binary collision between wet particles with the help of an analytical energy balance model, one needs to obtain closed-form expressions for losses of energy resulting from different forces involved in the collision. A closed-form expression for the solid-solid contact loss, independent of the contact force expression, will be presented in Section 2.3.4. However, information concerning the distances travelled by the colliding particles during the approach and separation stages is required to be integrated with the relevant expressions of the drag, buoyant, gravity, viscous, and capillary forces and help estimate the losses of energy due to these forces during a binary collision between wet particles. In addition, a robust evaluation algorithm for predicting the collision outcome should handle particles with different speeds. These conditions are present in many processing units, e.g., gas-solid fluidized beds. To satisfy these requirements, we (i) convert the particle velocities from the reference frame *I* into a new 1-D reference frame with respect to the center of mass (CM) of the colliding particles along $\vec{n}_{ij}$ and (ii) define a mobile unit vector $\vec{e}_x$ at the solid-solid contact position between the colliding particles directed to the center of the target particle *i* along the normal collision axis, as depicted in Fig. 2. The origin of $\vec{e}_x$ may be identical to, or different from, the CM of the hypothetical system under investigation. Note that, under certain circumstances, the CM of the colliding particles may be located between the center position and surface of the heavier particle involved in a binary particle collision. However, the origin of $\vec{e}_x$ is always located at the surface of the (much) heavier particle or between the surfaces of colliding particles. In Fig. 2, $\vec{u}_j$ is the velocity of the colliding neighbor particle *j* with respect to the reference frame *I*. $u_{i,\vec{n}_{ij}}$ and $u_{j,\vec{n}_{ij}}$ are the scalar projections of the velocities of particles *i* and *j* with respect to the reference frame *I* along $\vec{n}_{ij}$. v_i and v_j are the speeds of particles *i* and *j* with respect to the CM of the colliding particles along $\vec{n}_{ij}$ during the approach stage. l_{ie} and l_{je} are respectively the distances between the surfaces of particles *i* and *j* and the origin of $\vec{e}_x$ during the approach stage.

Referring to the assumption (xiv) in Section 2.1, one can expect that the CM of the colliding particles remains as an inertial frame of reference [46] during the approach stage. Since there is no relative movement between the origin of $\vec{e}_x$ and the CM of the colliding particles, the unit vector $\vec{e}_x$ can also be an inertial frame of reference during the approach stage. Therefore, the converted particle velocities from the reference frame *I* into the new 1-D reference frame with respect to the CM of the colliding particles along $\vec{n}_{ij}$ during the approach stage can also be reported on the basis of $\vec{e}_x$. Following the assumption (xv) in Section 2.1, an updated $\vec{u}_{CM,\vec{n}_{ij}}$ can be obtained at the end of the approach stage ($\vec{u}_{CM,app,\vec{n}_{ij}}$). From the conservation of momentum and instantaneous collision at the solid-solid contact point, assumption (xvi), $\vec{u}_{CM,\vec{n}_{ij}}$ remains constant (and equal to $\vec{u}_{CM,app,\vec{n}_{ij}}$) by the beginning of the separation stage. $\vec{u}_{CM,\vec{n}_{ij}}$ will also remain unvaried during the separation stage and prior to the end of this stage according to the assumption (xvii) in Section 2.1. Consequently, the particle velocities converted from the reference frame *I* into the new 1-D reference frame with respect to the CM of the colliding particles along $\vec{n}_{ij}$ during the separation stage can also be reported on the basis of $\vec{e}_x$.

Based on the above discussion, the position vector of the CM of the colliding particles *i* and *j*, $\vec{x}_{CM}$, and $\vec{u}_{CM,\vec{n}_{ij}}$ can be calculated as:

$$\vec{x}_{CM} = \left(\frac{m_{p,i}\ \vec{x}_i + m_{p,j}\ \vec{x}_j}{m_{p,i} + m_{p,j}} \right) \tag{6}$$

$$\vec{u}_{CM,\vec{n}_{ij}} = \left(\frac{m_{p,i}\ u_{i,\vec{n}_{ij}} + m_{p,j}\ u_{j,\vec{n}_{ij}}}{m_{p,i} + m_{p,j}} \right) \vec{n}_{ij} \tag{7}$$

where $m_{p,j}$ is the mass of wet particle *j*. Eq. (7) can be employed to estimate $\vec{u}_{0,CM,\vec{n}_{ij}}$ and $\vec{u}_{CM,app,\vec{n}_{ij}}$ as follows:

$$\vec{u}_{0,CM,\vec{n}_{ij}} = \left(\frac{m_{p,i}\ u_{0,i,\vec{n}_{ij}} + m_{p,j}\ u_{0,j,\vec{n}_{ij}}}{m_{p,i} + m_{p,j}} \right) \vec{n}_{ij} \tag{8}$$

$$\vec{u}_{CM,app,\vec{n}_{ij}} = \left(\frac{m_{p,i}\ u_{c,appi,\vec{n}_{ij}} + m_{p,j}\ u_{c,appj,\vec{n}_{ij}}}{m_{p,i} + m_{p,j}} \right) \vec{n}_{ij} \tag{9}$$

where $u_{0,i,\vec{n}_{ij}}$ and $u_{0,j,\vec{n}_{ij}}$ are respectively the scalar projections of the impact velocities of particles *i* and *j* with respect to the reference frame *I* along $\vec{n}_{ij}$. $u_{c,app,i,\vec{n}_{ij}}$ and $u_{c,app,j,\vec{n}_{ij}}$ are respectively the scalar projections of the velocities of particles *i* and *j* with respect to the reference frame *I* along $\vec{n}_{ij}$ at the end of the approach stage. The velocities of particles *i* and *j* with respect to the CM of the colliding particles along $\vec{n}_{ij}$ during the approach stage ($\vec{v}_i$ and $\vec{v}_j$, respectively) are defined as:

$$\vec{v}_i = u_{i,\vec{n}_{ij}}\vec{n}_{ij} - \vec{u}_{CM,\vec{n}_{ij}} = \frac{m_{p,j}}{m_{p,i} + m_{p,j}} u_{ij,\vec{n}_{ij}}\vec{n}_{ij} \tag{10}$$

$$\vec{v}_j = u_{j,\vec{n}_{ij}}\vec{n}_{ij} - \vec{u}_{CM,\vec{n}_{ij}} = -\frac{m_{p,i}}{m_{p,i} + m_{p,j}} u_{ij,\vec{n}_{ij}}\vec{n}_{ij} \tag{11}$$

where $u_{ij,\vec{n}_{ij}}$ is the scalar projection of the velocity of particle *i* relative to particle *j* with respect to the reference frame *I* along $\vec{n}_{ij}$ and is expressed by the following:

$$u_{ij,\overrightarrow{n}_{ij}} = u_{i,\overrightarrow{n}_{ij}} - u_{j,\overrightarrow{n}_{ij}} \tag{12}$$

Eqs. (10) and (11) can also be employed to estimate the velocities of particles i and j with respect to the CM of these colliding particles along $\overrightarrow{n}_{ij}$ during the separation stage ($\overrightarrow{\nu}_i$ and $\overrightarrow{\nu}_j$, respectively) when adopting the corresponding $\overrightarrow{u}_{CM,\overrightarrow{n}_{ij}}$ during the separation stage. With the help of the framework described above, if the kinetic energies of particles i and j are such that both particles reach the solid-solid contact point, while both were moving, or simultaneously stop before that, l_{ie} and l_{je} during the approach stage can be estimated as:

$$l_{ie} = \frac{v_i}{v_i + v_j} D \tag{13}$$

$$l_{je} = \frac{v_j}{v_i + v_j} D \tag{14}$$

Special cases where one particle stops moving prior to the solid-solid contact, while the other particle has some energy left to approach the stopped particle, will be discussed in Sections 2.3.5 and S-9 of the Supplementary Material. As alluded to earlier, D typically decreases from $h_{0,i} + h_{0,j}$ to $h_{a,i} + h_{a,j}$ during the approach stage. Integrating this information with Eqs. (13) and (14) allows us to estimate the distances travelled by the colliding particles during the approach stage. Similarly, if both particles i and j can pass the liquid bridge rupture point, while both were moving, or simultaneously stop prior to that condition during the separation stage, the distances between the surfaces of particles i and j and the origin of $\overrightarrow{e}_x$ during the separation stage (ℓ_{ie} and ℓ_{je}, respectively) can be obtained as:

$$\ell_{ie} = \frac{\nu_i}{\nu_i + \nu_j} D \tag{15}$$

$$\ell_{je} = \frac{\nu_j}{\nu_i + \nu_j} D \tag{16}$$

where ν_i and ν_j are the speeds of particles i and j with respect to the CM of the colliding particles along $\overrightarrow{n}_{ij}$ during the separation stage ($\nu_i = \left|\overrightarrow{\nu}_i\right|$ and $\nu_j = \left|\overrightarrow{\nu}_j\right|$). Special cases where one particle stops moving prior to the liquid bridge rupture point, while the other particle has some energy left to separate from the stopped particle, will be discussed in Sections S-11 and S-12 of the Supplementary Material. The distances travelled by the colliding particles during the separation stage can typically be estimated by Eqs. (15) and (16) since D often increases from $h_{a,i} + h_{a,j}$ to h_{rupt} during the separation stage. We need to convert the particle velocities from the reference frame I into a new 1-D reference frame with respect to the CM of the colliding particles along $\overrightarrow{n}_{ij}$ during either the approach or separation stage to establish a relevant theoretical background for the development of a generalized analytical energy balance agglomeration model. Eq. (5) can, hence, be reformulated based on the target particle velocity with respect to the CM of the colliding particles during the approach stage as follows:

$$m_{p,i}\frac{d\overrightarrow{v}_i}{dt} = \overrightarrow{F}_{cont,ij} + \overrightarrow{F}_{drag,i} + \overrightarrow{F}_{buoy,i} + \overrightarrow{W}_i + \overrightarrow{F}_{vis,i} + \overrightarrow{F}_{cap,i} \tag{17a}$$

or the CM of the colliding particles during the separation stage as follows:

$$m_{p,i}\frac{d\overrightarrow{\nu}_i}{dt} = \overrightarrow{F}_{cont,ij} + \overrightarrow{F}_{drag,i} + \overrightarrow{F}_{buoy,i} + \overrightarrow{W}_i + \overrightarrow{F}_{vis,i} + \overrightarrow{F}_{cap,i} \tag{17b}$$

The same treatment can be made for the general equation of motion of the colliding neighbor particle j during a sole binary wet collision with the target particle i (see Section S-2 of the Supplementary Material for details).

The expression proposed by Gidaspow [47] was adopted in this study to estimate the drag forces acting on the colliding particles. The vector of the drag force acting by the flowing gas on particle i can be calculated as [37,47]:

$$\overrightarrow{F}_{drag,i} = \begin{cases} \left(\dfrac{150\,(1-\varepsilon)}{\varepsilon\, {d_{p,i}}^2} \mu_g \left(\overrightarrow{u}_{g,i} - \overrightarrow{u}_i \right) + 1.75 \dfrac{\rho_g \left(\overrightarrow{u}_{g,i} - \overrightarrow{u}_i \right) \left| \overrightarrow{u}_{g,i} - \overrightarrow{u}_i \right|}{d_{p,i}} \right) V_{p,i} & \varepsilon < 0.80 \\ \dfrac{3}{4} C_{d,i} \rho_g \left(\overrightarrow{u}_{g,i} - \overrightarrow{u}_i \right) \left| \overrightarrow{u}_{g,i} - \overrightarrow{u}_i \right| \varepsilon^{-1.65} V_{p,i} \dfrac{1}{d_{p,i}} & \varepsilon \geq 0.80 \end{cases} \tag{18}$$

where ε is the local bed voidage, $d_{p,i}$ and $V_{p,i}$ are the diameter and volume of wet particle i, and $\overrightarrow{u}_{g,i}$ is the local gas velocity around particle i with respect to the reference frame I. μ_g and ρ_g are the gas viscosity and density, respectively, and $C_{d,i}$ is the drag coefficient for the isolated target particle i. $V_{p,i}$ and $C_{d,i}$ can be expressed as follows:

$$V_{p,i} = \frac{4}{3}\pi \left(r_{p,s,i} + h_{0,i} \right)^3 \tag{19}$$

$$C_{d,i} = \begin{cases} \frac{24}{Re_i}\left(1 + 0.15 Re_i^{0.687}\right) & Rei < 1000 \\ 0.44 & Re_i \geq 1000 \end{cases} \tag{20}$$

where Re_i is the Reynolds number of particle i. It is given by:

$$Re_i = \frac{\rho_g \varepsilon d_{p,i} \left| \vec{u}_{g,i} - \vec{u}_i \right|}{\mu_g} \tag{21}$$

In addition, the superficial gas velocity with respect to the reference frame I, $\vec{U}_g$, is correlated with the local gas and particle velocities with respect to the reference frame I ($\vec{u}_g$ and $\vec{u}$, respectively) and ε as [47]:

$$\vec{U}_g = \varepsilon\left(\vec{u}_g - \vec{u}\right) \tag{22}$$

If $\vec{u}_i$ in Eqs. (18) and (21) is substituted by the initial (impact) velocity of particle i with respect to the reference frame I, $\vec{u}_{0,i}$, $\vec{F}_{drag,i}$ at the impact condition is obtained. $\vec{F}_{buoy,i}$ and $\vec{W}_i$ can be calculated as follows:

$$\vec{F}_{buoy,i} = \rho_g V_{p,i} \vec{g} \tag{23}$$

$$\vec{W}_i = \frac{4\pi}{3}\left(\rho_{p,s,i} r_{p,s,i}^3 + \rho_l\left(\left(r_{p,s,i} + h_{0,i}\right)^3 - r_{p,s,i}^3\right)\right)\vec{g} \tag{24}$$

where $\vec{g}$ is the gravitational acceleration vector, $\rho_{p,s,i}$ is the density of solid particle i, and ρ_l is the liquid density. We can estimate the vector of the drag and buoyant forces acting on particle j ($\vec{F}_{drag,j}$ and $\vec{F}_{buoy,j}$, respectively), as well as the weight vector of particle j, $\vec{W}_j$, when employing the relevant parameters of this particle instead of those for particle i in Eqs. (18)–(21) and (23) and (24) (see Section S-2 of the Supplementary Material for details). We can calculate $\vec{F}_{cap,i}$ and $\vec{F}_{vis,i}$ (refer to the symbols defined in Fig. 1) based on the expressions proposed by Pitois et al. [36], which include the liquid bridge volume effect, and noting the Derjaguin approximation [38, 39] as follows:

$$\vec{F}_{cap,i} = 2\pi\gamma_l r_{p,s,ij} X_v \cos\theta \, \vec{e}_{n,i} \tag{25}$$

$$\vec{F}_{vis,i} = -\frac{3}{2}\pi\mu_l r_{p,s,ij}^2 X_v^2 \frac{\vec{v}_{ij}}{D} \tag{26a}$$

$$\vec{F}_{vis,i} = -\frac{3}{2}\pi\mu_l r_{p,s,ij}^2 X_v^2 \frac{\vec{v}_{ij}}{D} \tag{26b}$$

where μ_l and γ_l are the liquid viscosity and surface tension, X_v is the correction factor for the volume of the liquid bridge between two colliding wet particles, and $\vec{e}_{n,i}$ is the unit vector normal to the surface of particle i along the collision axis. $\vec{v}_{ij}$ and $\vec{v}_{ij}$ are the velocities of particle i relative to particle j with respect to the CM of the colliding particles along $\vec{n}_{ij}$ during the approach and separation stages, respectively. They can be defined as:

$$\vec{v}_{ij} = \vec{v}_i - \vec{v}_j \tag{27a}$$

$$\vec{v}_{ij} = \vec{v}_i - \vec{v}_j \tag{27b}$$

Note that $\vec{F}_{vis,i}$ always acts against the direction of the relative movement of the target particle i with respect to the colliding neighbor particle j along the axis of collision. The role of the negative signs in Eqs. (26a) and (26b) are to adjust the direction of $\vec{F}_{vis,i}$ with respect to $\vec{v}_{ij}$ and $\vec{v}_{ij}$. When the Derjaguin approximation can be adopted, the magnitudes of $\vec{F}_{cap,i}$ and $\vec{F}_{vis,i}$ are respectively the same as the magnitudes of the vector capillary and viscous forces acting on particle j ($\vec{F}_{cap,j}$ and $\vec{F}_{vis,j}$, respectively; see Section S-2 of the Supplementary Material for relevant expressions). However, in the treatment we adopted in this study, the magnitudes of the body forces acting on particle i are not identical to the magnitudes of the corresponding body forces acting on the colliding neighbor particle j when the colliding particles differ in size and/or mass. This is one of the main differences between this work and the modeling strategy adopted in the study by Balakin et al. [29], where they represented a system of unequal size and mass of particles with an equivalent system of equal size and mass for the sake of simplifying the analysis. While the Derjaguin approximation has been applied for systems of unequally sized particles having a small liquid bridge volume [39,48,49], it is not appropriate for the calculations of body forces.

Eq. (26) was derived on the basis of the lubrication (or thin film) approximation for a liquid bridge with finite volume between colliding wet particles. Details of this derivation are presented in Section S-3 of the Supplementary Material. X_v can be expressed by the

following:

$$X_v = 1 - \frac{D}{\sqrt{D^2 + a^2}} \tag{28}$$

where a^2 is a constant for a binary collision of wet particles, which is given by:

$$a^2 = \frac{2V_b}{\pi r_{p,s,ij}} \tag{29}$$

V_b in Eq. (29) is the volume of the liquid bridge between two wet particles and can be estimated by considering a cylindrical shape approximation for the liquid bridge connecting two particles as follows [2,40]:

$$V_b = \int_0^{r_w} 2\pi r\, H(r)\, dr = \frac{1}{2}\pi r_{p,s,ij}\left(H^2(r_w) - \left(h_{a,i} + h_{a,j}\right)^2\right) \tag{30}$$

2.3. Generalized agglomeration model

The evaluation of the outcome of a binary collision involving identical wet particles based on the analytical energy balance model proposed by Darabi et al. [2] was established on estimation of a wet (overall) restitution coefficient e_w. In the absence of rotation, e_w along the normal collision axis can be defined as follows:

$$e_w = \frac{\vec{u}_{r,sep,j,\vec{n}_{ij}} - \vec{u}_{r,sep,i,\vec{n}_{ij}}}{\vec{u}_{0,i,\vec{n}_{ij}} - \vec{u}_{0,j,\vec{n}_{ij}}} \tag{31}$$

where $\vec{u}_{r,sep,i,\vec{n}_{ij}}$ and $\vec{u}_{r,sep,j,\vec{n}_{ij}}$ are the velocities of the target particle i and colliding neighbor particle j with respect to the reference frame I along $\vec{n}_{ij}$ at the end of the separation stage, and $\vec{u}_{0,i,\vec{n}_{ij}}$ and $\vec{u}_{0,j,\vec{n}_{ij}}$ are the impact velocities of particles i and j with respect to the reference frame I along $\vec{n}_{ij}$. By neglecting the contributions of body forces in the evaluation of a binary collision outcome between identical wet particles, e_w was correlated with the actual total loss of energy during the collision incident and the total initial kinetic energy of the system. Please refer to Darabi et al. [2] and Shabanian et al. [31] for further details. To estimate the total loss of energy during the collision interval, Darabi et al. [2] proposed an approximate analytical approach to estimate viscous, capillary, and solid-solid contact losses and then combine them through the superposition principle. Since the general equation of motion, as described in Eq. (5), (17), or (S.1), has no analytical solution even when neglecting the body forces, Darabi et al. [2] recommended neglecting the capillary contribution in the equation of motion to obtain an analytical expression for the particle speed and, hence, expressions for the viscous and solid-solid contact losses. One can independently obtain an analytical expression for the loss of energy due to the capillary effect. They showed that the approximate analytical values obtained through the proposed analytical energy balance model were in good agreement with those attained by solving the equation of motion numerically. According to Darabi et al.'s model, two colliding identical wet particles agglomerate if $e_w = 0$, i.e., the maximum possible energy dissipation calculated by the analytical energy balance model is equal to or greater than the total initial kinetic energy of the system. Otherwise, a rebound outcome can take place and the corresponding e_w ($0 < e_w \leq e$) can be estimated.

We presented an improved version of Darabi et al.'s model [31]. In the improved model, referred to as the non-generalized model here, we evaluate the collision outcome in three steps based on the values of kinetic energy parameters rather than monitoring e_w. This allows the non-generalized model to be computationally more effective than Darabi et al.'s model, while a number of other critical advantages can be achieved by the model (see Shabanian et al. [31] for details). We followed a similar approach in the development of a generalized analytical energy balance model presented in this study. The new model (i) accounts for the collision of wet particles with different liquid layer thicknesses and solid particle properties, e.g., size, material, and asperity height, as well as initial/impact speeds and (ii) considers the effects of body forces, solid-solid contacting, and those of the liquid bridge volume-corrected capillary and viscous forces in predicting the outcome of a binary wet particle collision. Principal kinetic energy parameters to evaluate a collision outcome in the generalized model are the kinetic energies of particles i and j based on the converted particle velocities from the reference frame I to the 1-D reference frame with respect to the CM of the colliding particles along $\vec{n}_{ij}$ during the approach stage at the end of the approach stage ($K_{app,i}$ and $K_{app,j}$, respectively), as well as the kinetic energies of particles i and j based on the converted particle velocities from the reference frame I to a new reference frame with respect to the CM of the colliding particles along $\vec{n}_{ij}$ during the separation stage at the beginning of the separation stage ($\mathscr{K}_{sep,i}$ and $\mathscr{K}_{sep,j}$, respectively) and at the end of the separation stage ($\mathscr{K}_{fin,i}$ and $\mathscr{K}_{fin,j}$, respectively). We only considered the contribution of the viscous force (Eq. (26a) or (S.9a)) in Eq. (17a) or (S.1a) to obtain analytical expressions for the speeds of particles i and j during the approach stage and, hence, expressions for the viscous losses by these particles during this stage, as well as expressions for the solid-solid contact losses by these particles when considering the assumption (xvi) in Section 2.1. Likewise, we obtained analytical expressions for the speeds of particles i and j during the separation stage and, hence, expressions for their viscous losses during the same stage when solely considering the contribution of the viscous force (Eq. (26b) or (S.9b)) in Eq. (17b) or (S.1b). Analytical expressions for losses of energy due to the capillary effect by particles i and j during the approach and separation stages were obtained independently. The same procedure was followed for losses of energy due to the net effect of body forces acting on particles i and j during the approach and separation stages when considering the assumption (xii)

in Section 2.1. These energy loss terms, together with the initial kinetic energies of particles *i* and *j* based on the converted particle velocities from the reference frame *I* to the 1-D reference frame with respect to the CM of the colliding particles along $\vec{n}_{ij}$ during the approach stage ($K_{ini,i}$ and $K_{ini,j}$, respectively) form the basis for estimations of $K_{app,i}$, $K_{app,j}$, $\mathscr{K}_{sep,i}$, $\mathscr{K}_{sep,j}$, $\mathscr{K}_{fin,i}$, and $\mathscr{K}_{fin,j}$, thus the evaluation of a collision outcome through the generalized analytical energy balance model. Details on the expressions for the speeds of the particles and their losses of kinetic energy are provided in the next sections.

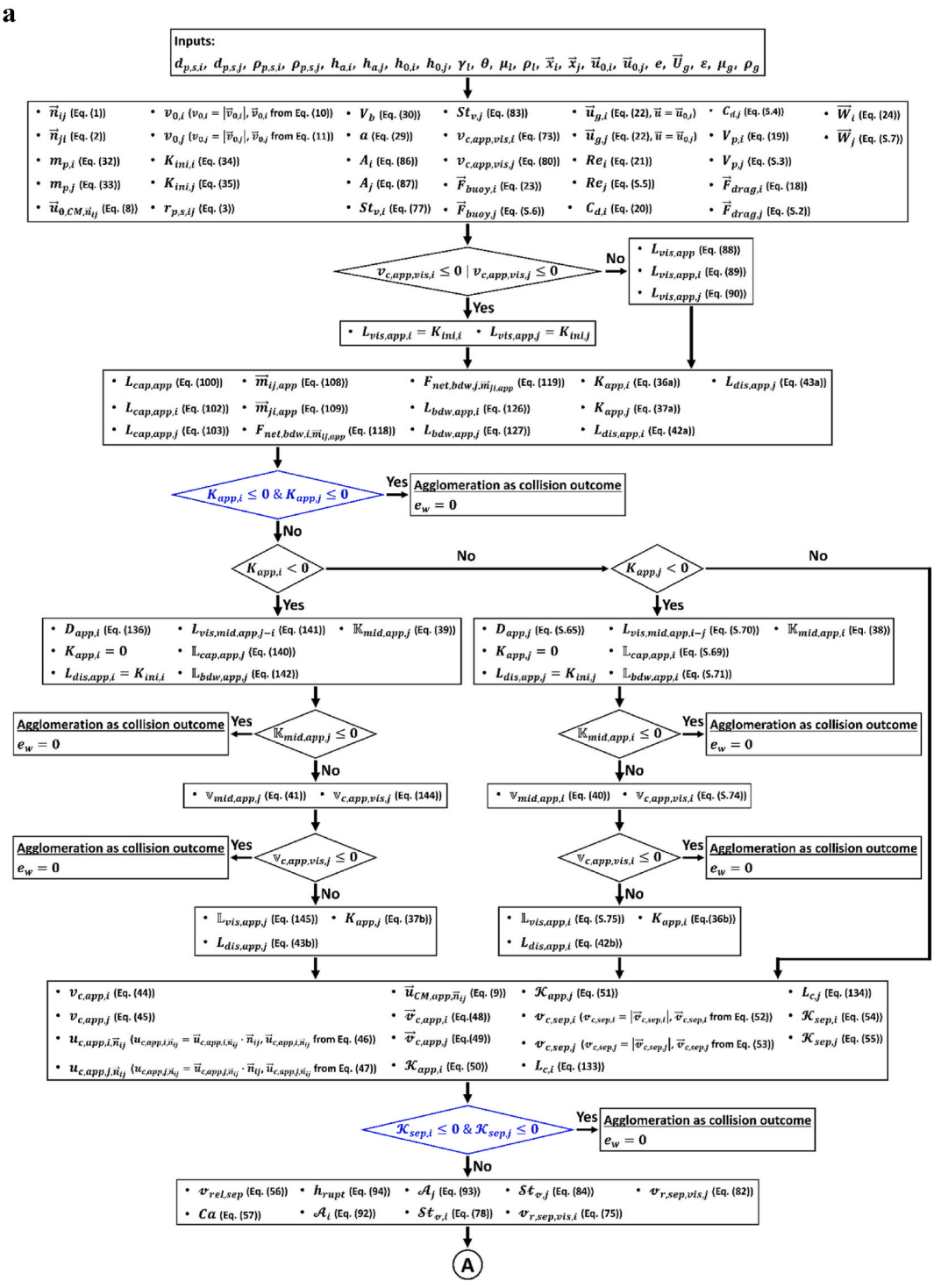

Fig. 3. Flow diagram of the generalized agglomeration model for a binary collision of wet particles. Remarks: (i) the evaluation order is top-to-bottom, and then left-to-right, and (ii) in some decision diamonds, "|" means "and/or", and "&" means "and".

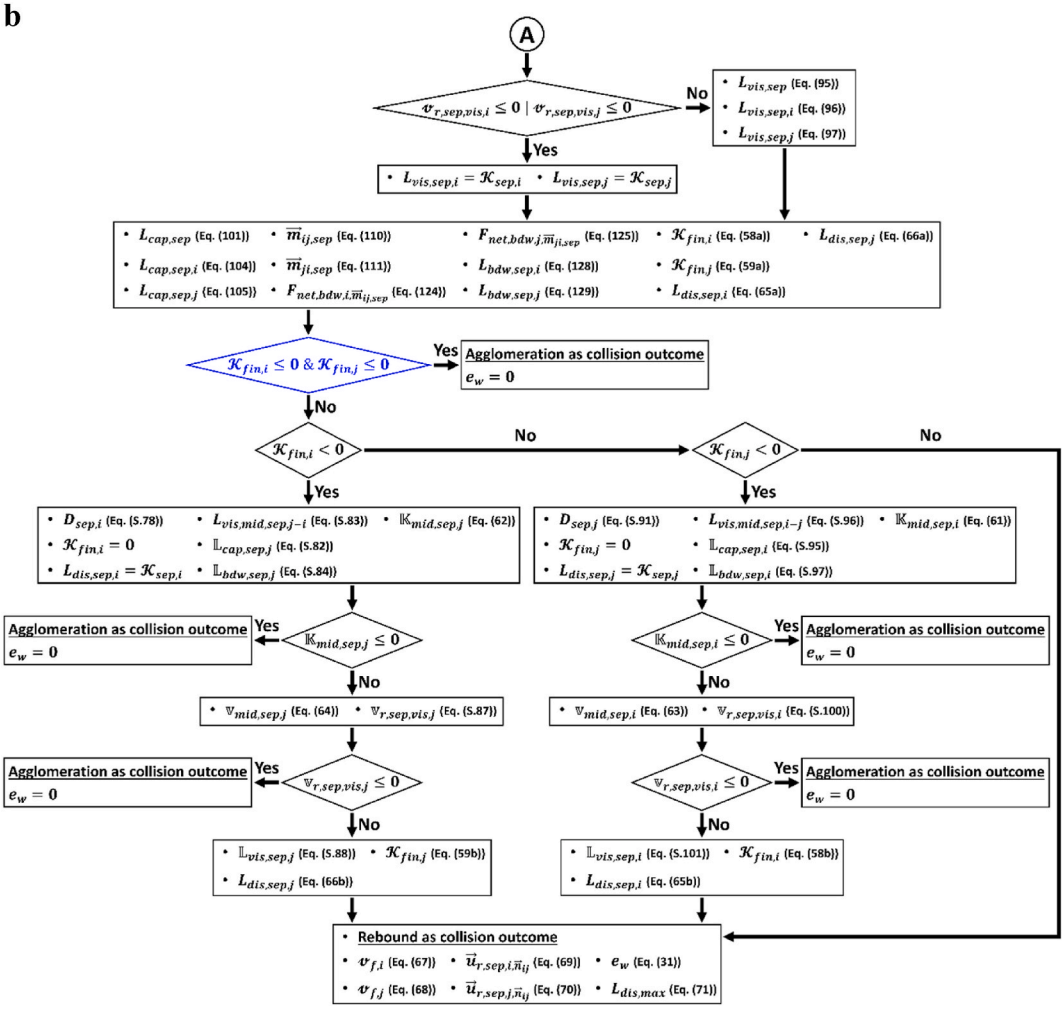

Fig. 3. (*continued*).

The flowchart of the generalized agglomeration model based on the analytical energy balance model for a binary collision of wet particles is presented in Fig. 3. According to this model, an agglomeration outcome can take place if one of the following conditions is satisfied: (i) $K_{app,i} \le 0$ and $K_{app,j} \le 0$, (ii) $\mathcal{K}_{sep,i} \le 0$ and $\mathcal{K}_{sep,j} \le 0$ or (iii) $\mathcal{K}_{fin,i} \le 0$ and $\mathcal{K}_{fin,j} \le 0$. These conditions respectively mean that total kinetic energies of colliding wet particles are dissipated during either the approach, solid-solid contact or separation stage. The calculations are terminated upon satisfying one of these conditions and a value of zero is assigned to e_w. If the conditions mentioned above are not satisfied, the remaining kinetic energies of the particles direct them toward the liquid bridge rupture, the colliding particles rebound and e_w can be estimated by Eq. (31). Special conditions may be experienced during either the approach or separation stage of a binary collision of non-identical wet particles, where one particle stops moving, while the other one can still continue its movement toward the solid-solid contact or liquid bridge rupture. The algorithm presented in Fig. 3 is capable of handling these situations via some kinetic energy parameters. The collision incident leads to particle agglomeration if the sole moving particle loses its kinetic energy before finishing the approach or separation stage, where the other particle has already lost its kinetic energy during that stage. Otherwise, the calculation will proceed toward the next stage of the collision or the end of the algorithm. Details of how we treat these special conditions will be discussed in Sections 2.3.5 and S-9 and S-11 of the Supplementary Material. Equations to calculate some parameters that are required for the algorithm presented in Fig. 3 are reported in Table 1.

In Fig. 3, $d_{p,s,j}$, $\rho_{p,s,j}$, $V_{p,j}$, $C_{d,j}$, Re_j, and $\overrightarrow{u}_{0,j}$ are respectively the diameter of the colliding neighbor solid particle j and its solid particle density, the volume of the wet particle j, the drag coefficient of the isolated particle j and its Reynolds number, as well as the impact velocity of particle j with respect to the reference frame I. $v_{0,i}$ and $v_{0,j}$ are the impact speeds of particles i and j with respect to the CM of the colliding particles along $\overrightarrow{n}_{ij}$ during the approach stage, respectively, while $\overrightarrow{v}_{0,i}$ and $\overrightarrow{v}_{0,j}$ are the impact velocities. A_i and A_j are constants, and $St_{v,i}$ and $St_{v,j}$ are the Stokes numbers of particles i and j defined based on the corresponding particle speed with respect to the mentioned frame of reference. $v_{c,app,vis,i}$ and $v_{c,app,vis,j}$ are the speeds of particles i and j with respect to the CM of the colliding particles along $\overrightarrow{n}_{ij}$ during the approach stage at the end of the approach stage, neglecting the effects of capillary and body forces. $L_{vis,app}$

Table 1
Additional equations to calculate parameters for a binary collision of wet particles introduced in Fig. 3.

$$m_{p,i} = \frac{4\pi}{3}(\rho_{p,s,i} r_{p,s,i}{}^3 + \rho_l((r_{p,s,i} + h_{0,i})^3 - r_{p,s,i}{}^3)) \quad (32)$$

$$m_{p,j} = \frac{4\pi}{3}(\rho_{p,s,j} r_{p,s,j}{}^3 + \rho_l((r_{p,s,j} + h_{0,j})^3 - r_{p,s,j}{}^3)) \quad (33)$$

$$K_{ini,i} = \frac{1}{2} m_{p,i} v_{0,i}{}^2 \quad (34)$$

$$K_{ini,j} = \frac{1}{2} m_{p,j} v_{0,j}{}^2 \quad (35)$$

$$K_{app,i} = K_{ini,i} - L_{cap,app,i} - L_{vis,app,i} - L_{bdw,app,i} \quad (36a)$$

$$K_{app,i} = K_{ini,i} - \mathbb{L}_{cap,app,i} - L_{vis,mid,app,i-j} - \mathbb{L}_{vis,app,i} - \mathbb{L}_{bdw,app,i} \quad (36b)$$

$$K_{app,j} = K_{ini,j} - L_{cap,app,j} - L_{vis,app,j} - L_{bdw,app,j} \quad (37a)$$

$$K_{app,j} = K_{ini,j} - \mathbb{L}_{cap,app,j} - L_{vis,mid,app,j-i} - \mathbb{L}_{vis,app,j} - \mathbb{L}_{bdw,app,j} \quad (37b)$$

$$\mathbb{K}_{mid,app,i} = K_{ini,i} - \mathbb{L}_{cap,app,i} - L_{vis,mid,app,i-j} - \mathbb{L}_{bdw,app,i} \quad (38)$$

$$\mathbb{K}_{mid,app,j} = K_{ini,j} - \mathbb{L}_{cap,app,j} - L_{vis,mid,app,j-i} - \mathbb{L}_{bdw,app,j} \quad (39)$$

$$\mathbb{v}_{mid,app,i} = \sqrt{2\mathbb{K}_{mid,app,i}/m_{p,i}} \quad (40)$$

$$\mathbb{v}_{mid,app,j} = \sqrt{2\mathbb{K}_{mid,app,j}/m_{p,j}} \quad (41)$$

$$L_{dis,app,i} = L_{cap,app,i} + L_{vis,app,i} + L_{bdw,app,i} \quad (42a)$$

$$L_{dis,app,i} = \mathbb{L}_{cap,app,i} + L_{vis,mid,app,i-j} + \mathbb{L}_{vis,app,i} + \mathbb{L}_{bdw,app,i} \quad (42b)$$

$$L_{dis,app,j} = L_{cap,app,j} + L_{vis,app,j} + L_{bdw,app,j} \quad (43a)$$

$$L_{dis,app,j} = \mathbb{L}_{cap,app,j} + L_{vis,mid,app,j-i} + \mathbb{L}_{vis,app,j} + \mathbb{L}_{bdw,app,j} \quad (43b)$$

$$v_{c,app,i} = \sqrt{2K_{app,i}/m_{p,i}} \quad (44)$$

$$v_{c,app,j} = \sqrt{2K_{app,j}/m_{p,j}} \quad (45)$$

$$\vec{u}_{c,app,i,\vec{n}_{ij}} = v_{c,app,i}\vec{n}_{ij} + \vec{u}_{0,CM,\vec{n}_{ij}} \quad (46)$$

$$\vec{u}_{c,app,j,\vec{n}_{ij}} = -v_{c,app,j}\vec{n}_{ij} + \vec{u}_{0,CM,\vec{n}_{ij}} \quad (47)$$

$$\vec{v}_{c,app,i} = u_{c,app,i,\vec{n}_{ij}}\vec{n}_{ij} - \vec{u}_{CM,app,\vec{n}_{ij}} \quad (48)$$

$$\vec{v}_{c,app,j} = u_{c,app,j,\vec{n}_{ij}}\vec{n}_{ij} - \vec{u}_{CM,app,\vec{n}_{ij}} \quad (49)$$

$$\mathcal{K}_{app,i} = \frac{1}{2} m_{p,i} v_{c,app,i}{}^2 \quad (50)$$

$$\mathcal{K}_{app,j} = \frac{1}{2} m_{p,j} v_{c,app,j}{}^2 \quad (51)$$

$$\vec{v}_{c,sep,i} = \frac{(m_{p,i} - em_{p,j})\vec{v}_{c,app,i} + m_{p,j}(1+e)\vec{v}_{c,app,j}}{m_{p,i} + m_{p,j}} \quad (52)$$

$$\vec{v}_{c,sep,j} = \frac{m_{p,i}(1+e)\vec{v}_{c,app,i} + (m_{p,j} - em_{p,i})\vec{v}_{c,app,j}}{m_{p,i} + m_{p,j}} \quad (53)$$

$$\mathcal{K}_{sep,i} = \frac{1}{2} m_{p,i} v_{c,sep,i}{}^2 \quad (54)$$

$$\mathcal{K}_{sep,j} = \frac{1}{2} m_{p,j} v_{c,sep,j}{}^2 \quad (55)$$

$$v_{rel,sep} = v_{c,sep,i} + v_{c,sep,j} \quad (56)$$

$$Ca = \mu_l v_{rel,sep}/\gamma_l \quad (57)$$

$$\mathcal{K}_{fin,i} = \mathcal{K}_{sep,i} - L_{cap,sep,i} - L_{vis,sep,i} - L_{bdw,sep,i} \quad (58a)$$

$$\mathcal{K}_{fin,i} = \mathcal{K}_{sep,i} - \mathbb{L}_{cap,sep,i} - L_{vis,mid,sep,i-j} - \mathbb{L}_{vis,sep,i} - \mathbb{L}_{bdw,sep,i} \quad (58b)$$

$$\mathcal{K}_{fin,j} = \mathcal{K}_{sep,j} - L_{cap,sep,j} - L_{vis,sep,j} - L_{bdw,sep,j} \quad (59a)$$

$$\mathcal{K}_{fin,j} = \mathcal{K}_{sep,j} - \mathbb{L}_{cap,sep,j} - L_{vis,mid,sep,j-i} - \mathbb{L}_{vis,sep,j} - \mathbb{L}_{bdw,sep,j} \quad (59b)$$

$$\mathbb{K}_{mid,sep,i} = \mathcal{K}_{sep,i} - \mathbb{L}_{cap,sep,i} - L_{vis,mid,sep,i-j} - \mathbb{L}_{bdw,sep,i} \quad (61)$$

$$\mathbb{K}_{mid,sep,j} = \mathcal{K}_{sep,j} - \mathbb{L}_{cap,sep,j} - L_{vis,mid,sep,j-i} - \mathbb{L}_{bdw,sep,j} \quad (62)$$

$$\mathbb{v}_{mid,sep,i} = \sqrt{2\mathbb{K}_{mid,sep,i}/m_{p,i}} \quad (63)$$

$$\mathbb{v}_{mid,sep,j} = \sqrt{2\mathbb{K}_{mid,sep,j}/m_{p,j}} \quad (64)$$

$$L_{dis,sep,i} = L_{cap,sep,i} + L_{vis,sep,i} + L_{bdw,sep,i} \quad (65a)$$

$$L_{dis,sep,i} = \mathbb{L}_{cap,sep,i} + L_{vis,mid,sep,i-j} + \mathbb{L}_{vis,sep,i} + \mathbb{L}_{bdw,sep,i} \quad (65b)$$

$$L_{dis,sep,j} = L_{cap,sep,j} + L_{vis,sep,j} + L_{bdw,sep,j} \quad (66a)$$

$$L_{dis,sep,j} = \mathbb{L}_{cap,sep,j} + L_{vis,mid,sep,j-i} + \mathbb{L}_{vis,sep,j} + \mathbb{L}_{bdw,sep,j} \quad (66b)$$

$$v_{f,i} = \sqrt{2\mathcal{K}_{fin,i}/m_{p,i}} \quad (67)$$

$$v_{f,j} = \sqrt{2\mathcal{K}_{fin,j}/m_{p,j}} \quad (68)$$

$$\vec{u}_{r,sep,i,\vec{n}_{ij}} = -v_{f,i}\vec{n}_{ij} + \vec{u}_{CM,app,i,\vec{n}_{ij}} \quad (69)$$

$$\vec{u}_{r,sep,j,\vec{n}_{ij}} = v_{f,j}\vec{n}_{ij} + \vec{u}_{CM,app,i,\vec{n}_{ij}} \quad (70)$$

$$L_{dis,max} = L_{dis,app,i} + L_{dis,app,j} + L_{c,i} + L_{c,j} + L_{dis,sep,i} + L_{dis,sep,j} \quad (71)$$

is the total loss of energy due to the viscous effect during the approach stage of a binary wet particle collision, while $L_{vis,app,i}$ and $L_{vis,app,j}$ are respectively the corresponding viscous losses for the particles i and j. $L_{cap,app}$ is the total loss of energy due to the capillary effect during the approach stage of a binary wet particle collision, while $L_{cap,app,i}$ and $L_{cap,app,j}$ are respectively the relevant capillary losses for particles i and j. $\vec{m}_{ij,app}$ is the unit vector along the velocity of particle i relative to particle j along the normal collision axis during the approach stage. Likewise, $\vec{m}_{ji,app}$ is the unit vector along the velocity of particle j relative to particle i along the normal collision axis during the approach stage. $F_{net,bdw,i,\vec{m}_{ij,app}}$ and $F_{net,bdw,j,\vec{m}_{ji,app}}$ are the scalar projections of the net of body forces acting on particle i along

$\vec{m}_{ij,app}$ and on particle j along $\vec{m}_{ji,app}$, respectively. $L_{bdw,app,i}$ and $L_{bdw,app,j}$ are respectively the losses of energy due to the net effect of buoyant, drag, and gravity forces for particles i and j during the approach stage. $L_{dis,app,i}$ and $L_{dis,app,j}$ are respectively the maximum possible energy dissipation calculated by the analytical energy balance model for particles i and j during the approach stage. $D_{app,i}$ is the distance D during the approach stage where the total kinetic energy of particle i is completely lost and $L_{vis,mid,app,j-i}$ is the loss of energy due to the viscous effect for particle j in the distance interval of $(h_{0,i} + h_{0,j})$ to $D_{app,i}$ during the approach stage. $\mathbb{L}_{cap,app,j}$ and $\mathbb{L}_{bdw,app,j}$ are the losses of energy due to the capillary effect and the net effect of body forces for particle j during the approach stage when particle i stops at $D_{app,i}$. $\mathbb{K}_{mid,app,j}$ is the kinetic energy of particle j based on the converted particle velocities from the reference frame I to the 1-D reference frame with respect to the CM of the colliding particles along $\vec{n}_{ij}$ during the approach stage at $D_{app,i}$, considering all losses of energy in the distance interval of $(h_{0,i} + h_{0,j})$ to $D_{app,i}$, as well as the losses of energy due to the capillary effect and the net effect of body forces in the distance interval of $D_{app,i}$ to $(h_{a,i} + h_{a,j})$. $D_{app,j}$ is the distance D during the approach stage where the total kinetic energy of particle j is completely lost and $L_{vis,mid,app,i-j}$ is the loss of energy due to the viscous effect for particle i in the distance interval of $(h_{0,i} + h_{0,j})$ to $D_{app,j}$ during the approach stage. $\mathbb{L}_{cap,app,i}$ and $\mathbb{L}_{bdw,app,i}$ are the losses of energy due to the capillary effect and the net effect of body forces for particle i during the approach stage when particle j stops at $D_{app,j}$. $\mathbb{K}_{mid,app,i}$ is the kinetic energy of particle i based on the converted particle velocities from the reference frame I to the 1-D reference frame with respect to the CM of the colliding particles along $\vec{n}_{ij}$ during the approach stage at $D_{app,j}$, considering all losses of energy in the distance interval of $(h_{0,i} + h_{0,j})$ to $D_{app,j}$, as well as the losses of energy due to the capillary effect and the net effect of body forces in the distance interval of $D_{app,j}$ to $(h_{a,i} + h_{a,j})$. $\mathbb{v}_{mid,app,j}$ is the speed of particle j with respect to the CM of the colliding particles along $\vec{n}_{ij}$ during the approach stage at $D_{app,i}$ (based on $\mathbb{K}_{mid,app,j}$). $\mathbb{v}_{c,app,vis,j}$ is the speed of particle j with respect to the CM of the colliding particles along $\vec{n}_{ij}$ during the approach stage at the end of the approach stage (based on $\mathbb{v}_{mid,app,j}$). $\mathbb{v}_{mid,app,i}$ is the speed of particle i with respect to the CM of the colliding particles along $\vec{n}_{ij}$ during the approach stage at $D_{app,j}$ (based on $\mathbb{K}_{mid,app,i}$). $\mathbb{v}_{c,app,vis,i}$ is the speed of particle i with respect to the CM of the colliding particles along $\vec{n}_{ij}$ during the approach stage at the end of the approach stage (based on $\mathbb{v}_{mid,app,i}$). $\mathbb{L}_{vis,app,j}$ is the loss of energy due to the viscous effect for particle j in the distance interval of $D_{app,i}$ to $(h_{a,i} + h_{a,j})$ during the approach stage. $\mathbb{L}_{vis,app,i}$ is the loss of energy due to the viscous effect for particle i in the distance interval of $D_{app,j}$ to $(h_{a,i} + h_{a,j})$ during the approach stage.

$v_{c,app,i}$ and $v_{c,app,j}$ are the speeds of particles i and j with respect to the CM of the colliding particles along $\vec{n}_{ij}$ during the approach stage at the end of the approach stage. $\vec{u}_{c,app,i,\vec{n}_{ij}}$ and $\vec{u}_{c,app,j,\vec{n}_{ij}}$ are the velocities of particles i and j with respect to the reference frame I along $\vec{n}_{ij}$ at the end of the approach stage. $\vec{v}_{c,app,i}$ and $\vec{v}_{c,app,j}$ are respectively the velocities of particles i and particle j with respect to the CM of the colliding particles along $\vec{n}_{ij}$ at the end of the approach stage. $\mathscr{K}_{app,i}$ and $\mathscr{K}_{app,j}$ are the kinetic energies of particles i and j based on the converted particle velocities from the reference frame I to a new reference frame with respect to the CM of the colliding particles along $\vec{n}_{ij}$ at the end of the approach stage. $v_{c,sep,i}$ and $v_{c,sep,j}$ are the speeds of particles i and j with respect to the CM of the colliding particles along $\vec{n}_{ij}$ during the separation stage at the beginning of the separation stage and $\vec{v}_{c,sep,i}$ and $\vec{v}_{c,sep,j}$ are the corresponding velocities. $L_{c,i}$ and $L_{c,j}$ are the contributions of particles i and j in the solid-solid contact loss between two wet particles. $v_{rel,sep}$ is the relative speed between the colliding particles i and j with respect to the CM of the colliding particles along $\vec{n}_{ij}$ during the separation stage at the beginning of the separation stage. Ca is the capillary number and $\mathscr{A}_i$ and $\mathscr{A}_j$ are constants. $\mathscr{St}_{v,i}$ and $\mathscr{St}_{v,j}$ are the Stokes numbers of particles i and j defined based on the corresponding particle speed with respect to the CM of the colliding particles along $\vec{n}_{ij}$ during the separation stage. $v_{r,sep,vis,i}$ and $v_{r,sep,vis,j}$ are the speeds of particles i and j with respect to the CM of the colliding particles along $\vec{n}_{ij}$ during the separation stage at the end of the separation stage, neglecting the effects of capillary and body forces during the separation stage.

$L_{vis,sep,i}$ and $L_{vis,sep,j}$ are respectively the losses of energy due to the viscous effect for particles i and j during the separation stage and $L_{vis,sep}$ is the corresponding total loss of energy. $L_{cap,sep,i}$ and $L_{cap,sep,j}$ are the losses of energy due to the capillary effect for particles i and j during the separation stage, respectively, and $L_{cap,sep}$ is the relevant total loss of energy. $\vec{m}_{ij,sep}$ is the unit vector along the velocity of particle i relative to particle j along the normal collision axis during the separation stage. $\vec{m}_{ji,sep}$ is the unit vector along the velocity of particle j relative to particle i along the normal collision axis during the separation stage. $F_{net,bdw,i,\vec{m}_{ij,sep}}$ and $F_{net,bdw,j,\vec{m}_{ji,sep}}$ are respectively the scalar projections of the net of body forces acting on particle i along $\vec{m}_{ij,sep}$ and on particle j along $\vec{m}_{ji,sep}$. $L_{bdw,sep,i}$ and $L_{bdw,sep,j}$ are the losses of energy due to the net effect of buoyant, drag, and gravity forces for particles i and j during the separation stage, respectively. $L_{dis,sep,i}$ and $L_{dis,sep,j}$ are the maximum possible energy dissipation calculated by the analytical energy balance model for particles i and j during the separation stage. $D_{sep,i}$ is the distance D during the separation stage where the total kinetic energy of particle i is completely lost and $L_{vis,mid,sep,j-i}$ is the loss of energy due to the viscous effect for particle j in the distance interval of $(h_{a,i} + h_{a,j})$ to $D_{sep,i}$ during the separation stage. $\mathbb{L}_{cap,sep,j}$ and $\mathbb{L}_{bdw,sep,j}$ are the losses of energy due to the capillary effect and the net effect of body forces for particle j during the separation stage when particle i stops at $D_{sep,i}$. $\mathbb{K}_{mid,sep,j}$ is the kinetic energy of particle j based on the converted particle velocities from the reference frame I to the 1-D reference frame with respect to the CM of the colliding particles along $\vec{n}_{ij}$ during the separation stage at $D_{sep,i}$, considering all losses of energy in the distance interval of $(h_{a,i} + h_{a,j})$ to $D_{sep,i}$, as well as the losses of energy due to the capillary effect and the net effect of body forces in the distance interval of $D_{sep,i}$ to h_{rupt}. $D_{sep,j}$ is the distance D during the separation stage where the total kinetic energy of particle j is completely lost and $L_{vis,mid,sep,i-j}$ is the loss of energy due to the viscous effect for particle i in the distance interval of $(h_{a,i} + h_{a,j})$ to $D_{sep,j}$ during the separation stage. $\mathbb{L}_{cap,sep,i}$ and $\mathbb{L}_{bdw,sep,i}$ are the losses of energy due to the capillary effect and the net effect of body forces for particle i during the separation stage when particle j stops at $D_{sep,j}$.

$\mathbb{K}_{mid,sep,i}$ is the kinetic energy of particle i based on the converted particle velocities from the reference frame I to the 1-D reference frame with respect to CM of the colliding particles along $\overrightarrow{n}_{ij}$ during the separation stage at $D_{sep,j}$, considering all losses of energy in the distance interval of $(h_{a,i}+h_{a,j})$ to $D_{sep,j}$, as well as the losses of energy due to the capillary effect and the net effect of body forces in the distance interval of $D_{sep,j}$ to h_{rupt}. $\mathbb{v}_{mid,sep,j}$ is the speed of particle j with respect to the CM of the colliding particles along $\overrightarrow{n}_{ij}$ during the separation stage at $D_{sep,i}$ (based on $\mathbb{K}_{mid,sep,j}$). $\mathbb{v}_{r,sep,vis,j}$ is the speed of particle j with respect to the CM of the colliding particles along $\overrightarrow{n}_{ij}$ during the separation stage at the end of the separation stage (based on $\mathbb{v}_{mid,sep,j}$). $\mathbb{v}_{mid,sep,i}$ is the speed of particle i with respect to the CM of the colliding particles along $\overrightarrow{n}_{ij}$ during the separation stage at $D_{sep,j}$ (based on $\mathbb{K}_{mid,sep,i}$). $\mathbb{v}_{r,sep,vis,i}$ is the speed of particle i with respect to the CM of the colliding particles along $\overrightarrow{n}_{ij}$ during the separation stage at the end of the separation stage (based on $\mathbb{v}_{mid,sep,i}$). $\mathbb{L}_{vis,sep,i}$ is the loss of energy due to the viscous effect for particle i in the distance interval of $D_{sep,j}$ to h_{rupt} during the separation stage. $\mathbb{L}_{vis,sep,j}$ is the loss of energy due to the viscous effect for particle j in the distance interval of $D_{sep,i}$ to h_{rupt} during the separation stage. $\mathscr{v}_{f,i}$ and $\mathscr{v}_{f,j}$ are the speeds of particles i and j with respect to the CM of the colliding particles along $\overrightarrow{n}_{ij}$ during the separation stage at the end of the separation stage. $L_{dis,max}$ is the maximum possible energy dissipation calculated by the analytical energy balance model for a binary collision of wet particles.

2.3.1. Loss of energy due to the viscous effect

To obtain analytical expressions for the total and individual losses of energy due to the viscous effect for the target particle i and colliding neighbor particle j during the approach and separation stages, we need to integrate the corresponding viscous force expressions over the hypothetically travelled distances during these stages. To reach this, we need to first obtain the relevant particle speed expressions during the approach and separation stages as, according to Eqs. (26) and (S-9), the viscous force varies with the particle velocity. These expressions will also be adopted to determine $v_{c,app,i}$ and $v_{c,app,j}$, which will be required for estimation of the solid-solid contact loss. Substituting Eq. (26a) into Eq. (17a), and converting the resulting equation from the vector form into the scalar form results in the expressions for the approach speed of particle i with respect to the CM of the colliding particles during the approach stage, neglecting the effects of capillary and body forces ($v_{app,vis,i}$ and $v_{c,app,vis,i}$). Following the same procedure, when substituting Eq. (26b) into Eq. (17b), we can obtain the separation speed of particle i with respect to the CM of the colliding particles during the separation stage, neglecting the effects of capillary and body forces during the separation stage ($\mathscr{v}_{sep,vis,i}$ and $\mathscr{v}_{r,sep,vis,i}$). These speeds can be expressed as follows (see Section S-4 of the Supplementary Material for details):

$$v_{app,vis,i}=\begin{cases} v_{0,i}\left(1-\dfrac{1}{St_{v,i}}\ln\left(\dfrac{f\left(h_{0,i}+h_{0,j}\right)}{f(D)}\right)\right), & St_{v,i}>\ln\left(\dfrac{f\left(h_{0,i}+h_{0,j}\right)}{f(D)}\right)\\ 0, & St_{v,i}\le\ln\left(\dfrac{f\left(h_{0,i}+h_{0,j}\right)}{f(D)}\right)\end{cases} \tag{72}$$

$$v_{c,app,vis,i}=\begin{cases} v_{0,i}\left(1-\dfrac{1}{St_{v,i}}\ln\left(\dfrac{f\left(h_{0,i}+h_{0,j}\right)}{f\left(h_{a,i}+h_{a,j}\right)}\right)\right), & St_{v,i}>\ln\left(\dfrac{f\left(h_{0,i}+h_{0,j}\right)}{f\left(h_{a,i}+h_{a,j}\right)}\right)\\ 0, & St_{v,i}\le\ln\left(\dfrac{f\left(h_{0,i}+h_{0,j}\right)}{f\left(h_{a,i}+h_{a,j}\right)}\right)\end{cases} \tag{73}$$

$$\mathscr{v}_{sep,vis,i}=\begin{cases} \mathscr{v}_{c,sep,i}\left(1-\dfrac{1}{\mathscr{St}_{e,i}}\ln\left(\dfrac{f(D)}{f\left(h_{a,i}+h_{a,j}\right)}\right)\right), & \mathscr{St}_{e,i}>\ln\left(\dfrac{f(D)}{f\left(h_{a,i}+h_{a,j}\right)}\right)\\ 0, & \mathscr{St}_{e,i}\le\ln\left(\dfrac{f(D)}{f\left(h_{a,i}+h_{a,j}\right)}\right)\end{cases} \tag{74}$$

$$\mathscr{v}_{r,sep,vis,i}=\begin{cases} \mathscr{v}_{c,sep,i}\left(1-\dfrac{1}{\mathscr{St}_{e,i}}\ln\left(\dfrac{f\left(h_{rupt}\right)}{f\left(h_{a,i}+h_{a,j}\right)}\right)\right), & \mathscr{St}_{e,i}>\ln\left(\dfrac{f\left(h_{rupt}\right)}{f\left(h_{a,i}+h_{a,j}\right)}\right)\\ 0, & \mathscr{St}_{e,i}\le\ln\left(\dfrac{f\left(h_{rupt}\right)}{f\left(h_{a,i}+h_{a,j}\right)}\right)\end{cases} \tag{75}$$

where $f(D)$ is a distance function for a binary collision of wet particles, which is defined as:

$$f(D)=\frac{D\sqrt{D^2+a^2}}{\left(D+\sqrt{D^2+a^2}\right)^2} \tag{76}$$

In addition, $St_{v,i}$ and $\mathscr{St}_{e,i}$ are given by:

$$St_{v,i}=\frac{2m_{p,i}v_{0,i}}{3\pi\mu_l r_{p,s,ij}^{\,2}} \tag{77}$$

$$\mathscr{St}_{\epsilon,i}=\frac{2m_{p,i}\epsilon'_{c,sep,i}}{3\pi\mu_l r_{p,s,ij}{}^2} \tag{78}$$

We can obtain the analogous expressions for the approach speed of particle j with respect to the CM of the colliding particles during the approach stage, neglecting the effects of capillary and body forces ($v_{app,vis,j}$ and $v_{c,app,vis,j}$) by repeating the same procedure described above and substituting Eq. (S.9a) into Eq. (S.1a). Similarly, we can obtain the expressions for the separation speed of particle j with respect to the CM of the colliding particles during the separation stage, neglecting the effects of capillary and body forces during the separation stage ($\epsilon'_{sep,vis,j}$ and $\epsilon'_{r,sep,vis,j}$), by substituting Eq. (S.9b) into Eq. (S.1b). The expressions for these speeds can be reported as follows (see Section S-4 ofthe Supplementary Material for details):

$$v_{app,vis,j}=\begin{cases} v_{0,j}\left(1-\dfrac{1}{St_{v,j}}\ln\left(\dfrac{f\left(h_{0,i}+h_{0,j}\right)}{f(D)}\right)\right), & St_{v,j}>\ln\left(\dfrac{f\left(h_{0,i}+h_{0,j}\right)}{f(D)}\right) \\ 0, & St_{v,j}\le\ln\left(\dfrac{f\left(h_{0,i}+h_{0,j}\right)}{f(D)}\right) \end{cases} \tag{79}$$

$$v_{c,app,vis,j}=\begin{cases} v_{0,j}\left(1-\dfrac{1}{St_{v,j}}\ln\left(\dfrac{f\left(h_{0,i}+h_{0,j}\right)}{f\left(h_{a,i}+h_{a,j}\right)}\right)\right), & St_{v,j}>\ln\left(\dfrac{f\left(h_{0,i}+h_{0,j}\right)}{f\left(h_{a,i}+h_{a,j}\right)}\right) \\ 0, & St_{v,j}\le\ln\left(\dfrac{f\left(h_{0,i}+h_{0,j}\right)}{f\left(h_{a,i}+h_{a,j}\right)}\right) \end{cases} \tag{80}$$

$$\epsilon'_{sep,vis,j}=\begin{cases} \epsilon'_{c,sep,j}\left(1-\dfrac{1}{\mathscr{St}_{\epsilon,j}}\ln\left(\dfrac{f(D)}{f\left(h_{a,i}+h_{a,j}\right)}\right)\right), & \mathscr{St}_{\epsilon,j}>\ln\left(\dfrac{f(D)}{f\left(h_{a,i}+h_{a,j}\right)}\right) \\ 0, & \mathscr{St}_{\epsilon,j}\le\ln\left(\dfrac{f(D)}{f\left(h_{a,i}+h_{a,j}\right)}\right) \end{cases} \tag{81}$$

$$\epsilon'_{r,sep,vis,j}=\begin{cases} \epsilon'_{c,sep,j}\left(1-\dfrac{1}{\mathscr{St}_{\epsilon,j}}\ln\left(\dfrac{f\left(h_{rupt}\right)}{f\left(h_{a,i}+h_{a,j}\right)}\right)\right), & \mathscr{St}_{\epsilon,j}>\ln\left(\dfrac{f\left(h_{rupt}\right)}{f\left(h_{a,i}+h_{a,j}\right)}\right) \\ 0, & \mathscr{St}_{\epsilon,j}\le\ln\left(\dfrac{f\left(h_{rupt}\right)}{f\left(h_{a,i}+h_{a,j}\right)}\right) \end{cases} \tag{82}$$

where $St_{v,j}$ and $\mathscr{St}_{\epsilon,j}$ are estimated by:

$$St_{v,j}=\frac{2m_{p,j}v_{0,j}}{3\pi\mu_l r_{p,s,ij}{}^2} \tag{83}$$

$$\mathscr{St}_{\epsilon,j}=\frac{2m_{p,j}\epsilon'_{c,sep,j}}{3\pi\mu_l r_{p,s,ij}{}^2} \tag{84}$$

Since we adopted the Derjaguin approximation in this study to describe the liquid bridge-induced interparticle forces between the colliding wet particles, the magnitudes of $\overrightarrow{F}_{vis,i}$ and $\overrightarrow{F}_{vis,j}$ are the same in this treatment. Hence, we can employ either of these vector forces with the corresponding particle speed expression, Eq. (26a) with Eq. (72) or Eq. (S.9a) with Eq. (79), to calculate the total work done by the liquid bridge on the colliding wet particles due to the viscous force during the approach stage of the binary wet particle collision $W_{vis,app}$ as follows (see Section S-4 of the Supplementary Material for details):

$$W_{vis,app}=\int_{h_{0,i}+h_{0,j}}^{h_{a,i}+h_{a,j}}\overrightarrow{F}_{vis,i}\bullet\left(\overrightarrow{e}_x\,dD\right)=-\left(A_i+A_j\right)\ln\left(\frac{f\left(h_{0,i}+h_{0,j}\right)}{f\left(h_{a,i}+h_{a,j}\right)}\right)-\left(\frac{A_i}{2St_{v,i}}+\frac{A_j}{2St_{v,j}}\right)\left[ln^2\left(f\left(h_{0,i}+h_{0,j}\right)\right)-ln^2\left(f\left(h_{a,i}+h_{a,j}\right)\right)\right.$$
$$\left.-2\ln\left(f\left(h_{0,i}+h_{0,j}\right)\right)\ln\left(\frac{f\left(h_{0,i}+h_{0,j}\right)}{f\left(h_{a,i}+h_{a,j}\right)}\right)\right] \tag{85}$$

where constants A_i and A_j are given by:

$$A_i=\frac{3}{2}\pi\mu_l r_{p,s,ij}{}^2 v_{0,i} \tag{86}$$

$$A_j=\frac{3}{2}\pi\mu_l r_{p,s,ij}{}^2 v_{0,j} \tag{87}$$

Referring to the assumption (xviii) in Section 2.1, if we describe the collision incident by the first law of thermodynamics while considering the control surface around the penetrating wet particles into the liquid bridge, the total work done by the colliding wet

particles on their surrounding liquid bridge is $-W_{vis,app}$. Therefore, $L_{vis,app}$ can be expressed as follows:

$$L_{vis,app} = -W_{vis,app} = (A_i + A_j)\ln\left(\frac{f(h_{0,i}+h_{0,j})}{f(h_{a,i}+h_{a,j})}\right) + \left(\frac{A_i}{2St_{v,i}} + \frac{A_j}{2St_{v,j}}\right)\left[ln^2\left(f(h_{0,i}+h_{0,j})\right) - ln^2\left(f(h_{a,i}+h_{a,j})\right) - 2\ln\left(f(h_{0,i}+h_{0,j})\right)\ln\left(\frac{f(h_{0,i}+h_{0,j})}{f(h_{a,i}+h_{a,j})}\right)\right] \quad (88)$$

If both particles i and j have enough kinetic energy to reach the solid-solid contact point, since $\left|\overrightarrow{F}_{vis,i}\right| = \left|\overrightarrow{F}_{vis,j}\right|$ based on the Derjaguin approximation, $L_{vis,app,i}$ and $L_{vis,app,j}$ can be estimated based on $L_{vis,app}$ and the distance portion travelled by particles i and j during the approach stage. The distance portion travelled by particles i and j during the approach stage can be related to v_i and v_j based on Eqs. (13) and (14) under conditions of interest here. According to the assumption (xiv) in Section 2.1, the particle speed ratios appeared in Eqs. (13) and (14) can also be reported based on $v_{0,i}$ and $v_{0,j}$ to obtain the distance portion travelled by particles i and j during the approach stage. Thus, $L_{vis,app,i}$ and $L_{vis,app,j}$ can be calculated as:

$$L_{vis,app,i} = \frac{v_{0,i}}{v_{0,i}+v_{0,j}}L_{vis,app} = \frac{v_{0,i}}{v_{0,i}+v_{0,j}}\left[(A_i + A_j)\ln\left(\frac{f(h_{0,i}+h_{0,j})}{f(h_{a,i}+h_{a,j})}\right) + \left(\frac{A_i}{2St_{v,i}} + \frac{A_j}{2St_{v,j}}\right)\left[ln^2\left(f(h_{0,i}+h_{0,j})\right) - ln^2\left(f(h_{a,i}+h_{a,j})\right) - 2\ln\left(f(h_{0,i}+h_{0,j})\right)\ln\left(\frac{f(h_{0,i}+h_{0,j})}{f(h_{a,i}+h_{a,j})}\right)\right]\right] \quad (89)$$

$$L_{vis,app,j} = \frac{v_{0,j}}{v_{0,i}+v_{0,j}}L_{vis,app} = \frac{v_{0,j}}{v_{0,i}+v_{0,j}}\left[(A_i + A_j)\ln\left(\frac{f(h_{0,i}+h_{0,j})}{f(h_{a,i}+h_{a,j})}\right) + \left(\frac{A_i}{2St_{v,i}} + \frac{A_j}{2St_{v,j}}\right)\left[ln^2\left(f(h_{0,i}+h_{0,j})\right) - ln^2\left(f(h_{a,i}+h_{a,j})\right) - 2\ln\left(f(h_{0,i}+h_{0,j})\right)\ln\left(\frac{f(h_{0,i}+h_{0,j})}{f(h_{a,i}+h_{a,j})}\right)\right]\right] \quad (90)$$

If particles i and j simultaneously stop prior to the solid-solid contact point, we can calculate $L_{vis,app,i}$ and $L_{vis,app,j}$ with Eqs. (89) and (90), respectively, when replacing $(h_{a,i} + h_{a,j})$ by a relevant D in these equations. It is shown in Section S-5 of the Supplementary Material that the initial kinetic energies of the colliding particles are totally dissipated by the corresponding viscous losses of energy for these particles during the approach stage if $v_{c,app,vis,i} \leq 0$ and/or $v_{c,app,vis,j} \leq 0$. With a similar approach to what was explained for $W_{vis,app}$, we can employ either of $\overrightarrow{F}_{vis,i}$ or $\overrightarrow{F}_{vis,j}$ with the corresponding particle speed expression during the separation stage, Eq. (26b) with Eq. (74) or Eq. (S.9b) with Eq. (81), to estimate the total work done by the liquid bridge on the colliding wet particles due to the viscous force during the separation stage of the binary wet particle collision $W_{vis,sep}$ as follows (see Section S-4 of the Supplementary Material for details):

$$W_{vis,sep} = \int_{h_{a,i}+h_{a,j}}^{h_{rupt}} \overrightarrow{F}_{vis,i} \bullet \left(\overrightarrow{e}_x\, dD\right) = -(\mathscr{A}_i + \mathscr{A}_j)\ln\left(\frac{f(h_{rupt})}{f(h_{a,i}+h_{a,j})}\right) + \left(\frac{\mathscr{A}_i}{2\mathscr{S}\ell_{e,i}} + \frac{\mathscr{A}_j}{2\mathscr{S}\ell_{e,j}}\right)\left[ln^2\left(f(h_{rupt})\right) - ln^2\left(f(h_{a,i}+h_{a,j})\right) - 2\ln\left(f(h_{a,i}+h_{a,j})\right)\ln\left(\frac{f(h_{rupt})}{f(h_{a,i}+h_{a,j})}\right)\right] \quad (91)$$

where constants $\mathscr{A}_i$ and $\mathscr{A}_j$ are given by:

$$\mathscr{A}_i = \frac{3}{2}\pi\mu_l r_{p,s,ij}{}^2 \ell_{c,sep,i} \quad (92)$$

$$\mathscr{A}_j = \frac{3}{2}\pi\mu_l r_{p,s,ij}{}^2 \ell_{c,sep,j} \quad (93)$$

We employ the correlation proposed by Pitois et al. [36] to estimate h_{rupt} under both static and dynamic conditions. It is given by:

$$h_{rupt} = \left(1 + \frac{\theta}{2}\right)\left(1 + Ca^{1/2}\right)V_b{}^{1/3} \quad (94)$$

Ideally, we need to utilize the relative speed between the colliding particles at the liquid bridge rupture point to estimate h_{rupt} by Eq. (94). This requires an iterative calculation. However, as done by Balakin et al. [29] and in our earlier study [31], we employ $\ell_{rel,sep}$, which yields a slight overestimation of h_{rupt}. Adopting the above-mentioned thermodynamic analogy, $L_{vis,sep}$ can be calculated as follows:

$$L_{vis,sep} = -W_{vis,sep} = (\mathscr{A}_i + \mathscr{A}_j)\ln\left(\frac{f(h_{rupt})}{f(h_{a,i}+h_{a,j})}\right) - \left(\frac{\mathscr{A}_i}{2\mathscr{S}\ell_{e,i}} + \frac{\mathscr{A}_j}{2\mathscr{S}\ell_{e,j}}\right)\left[ln^2(f(h_{rupt})) - ln^2(f(h_{a,i}+h_{a,j})) - 2\ln(f(h_{a,i}+h_{a,j}))\ln\left(\frac{f(h_{rupt})}{f(h_{a,i}+h_{a,j})}\right)\right] \quad (95)$$

If both colliding wet particles i and j can reach the liquid bridge rupture point, considering the remarks mentioned above for the calculations of $L_{vis,app,i}$ and $L_{vis,app,j}$, Eqs. (15) and (16), and the assumption (xvii) in Section 2.1, $L_{vis,sep,i}$ and $L_{vis,sep,j}$ can be defined as follows:

$$L_{vis,sep,i} = \frac{\mathscr{V}_{c,sep,i}}{\mathscr{V}_{c,sep,i}+\mathscr{V}_{c,sep,j}}L_{vis,sep} = \frac{\mathscr{V}_{c,sep,i}}{\mathscr{V}_{c,sep,i}+\mathscr{V}_{c,sep,j}}\left[(\mathscr{A}_i+\mathscr{A}_j)\ln\left(\frac{f(h_{rupt})}{f(h_{a,i}+h_{a,j})}\right) - \left(\frac{\mathscr{A}_i}{2\mathscr{S}\ell_{e,i}}+\frac{\mathscr{A}_j}{2\mathscr{S}\ell_{e,j}}\right)\left[ln^2(f(h_{rupt})) - ln^2(f(h_{a,i}+h_{a,j})) - 2\ln(f(h_{a,i}+h_{a,j}))\ln\left(\frac{f(h_{rupt})}{f(h_{a,i}+h_{a,j})}\right)\right]\right] \quad (96)$$

$$L_{vis,sep,j} = \frac{\mathscr{V}_{c,sep,j}}{\mathscr{V}_{c,sep,i}+\mathscr{V}_{c,sep,j}}L_{vis,sep} = \frac{\mathscr{V}_{c,sep,j}}{\mathscr{V}_{c,sep,i}+\mathscr{V}_{c,sep,j}}\left[(\mathscr{A}_i+\mathscr{A}_j)\ln\left(\frac{f(h_{rupt})}{f(h_{a,i}+h_{a,j})}\right) - \left(\frac{\mathscr{A}_i}{2\mathscr{S}\ell_{e,i}}+\frac{\mathscr{A}_j}{2\mathscr{S}\ell_{e,j}}\right)\left[ln^2(f(h_{rupt})) - ln^2(f(h_{a,i}+h_{a,j})) - 2\ln(f(h_{a,i}+h_{a,j}))\ln\left(\frac{f(h_{rupt})}{f(h_{a,i}+h_{a,j})}\right)\right]\right] \quad (97)$$

If particles i and j simultaneously stop prior to the liquid bridge rupture point during the separation stage, $L_{vis,sep,i}$ and $L_{vis,sep,j}$ can be respectively calculated by Eqs. (96) and (97), while replacing h_{rupt} by a relevant D in these equations. It is demonstrated in Section S-6 of the Supplementary Material that the energy losses by the viscous effect for the colliding particles during the separation stage could dissipate the kinetic energy that they possessed at the beginning of the separation stage if $\mathscr{V}_{r,sep,vis,i} \leq 0$ and/or $\mathscr{V}_{r,sep,vis,j} \leq 0$.

2.3.2. Loss of energy due to the capillary effect

Since $\left|\vec{F}_{cap,i}\right| = \left|\vec{F}_{cap,j}\right|$ according to the Derjaguin approximation, the total work done by the liquid bridge on the colliding wet particles due to the capillary force during the approach and separation stages of a binary wet particle collision ($W_{cap,app}$ and $W_{cap,sep}$, respectively) can be estimated based either on Eq. (25) or (S.8) as follows (see Section S-7 of the Supplementary Material for details):

$$W_{cap,app} = \int_{h_{0,i}+h_{0,j}}^{h_{a,i}+h_{a,j}} \vec{F}_{cap,i} \bullet \left(\vec{e}_x\, dD\right) = \int_{h_{0,i}+h_{0,j}}^{h_{a,i}+h_{a,j}} \vec{F}_{cap,j} \bullet \left(-\vec{e}_x\right) dD = 2\pi\gamma_l r_{p,s,ij}\cos\theta\left[\left((h_{0,i}+h_{0,j}) - \sqrt{(h_{0,i}+h_{0,j})^2+a^2}\right) - \left((h_{a,i}+h_{a,j}) - \sqrt{(h_{a,i}+h_{a,j})^2+a^2}\right)\right] \quad (98)$$

$$W_{cap,sep} = \int_{h_{a,i}+h_{a,j}}^{h_{rupt}} \vec{F}_{cap,i} \bullet \left(\vec{e}_x\, dD\right) = \int_{h_{a,i}+h_{a,j}}^{h_{rupt}} \vec{F}_{cap,j} \bullet \left(-\vec{e}_x\right) dD = -2\pi\gamma_l r_{p,s,ij}\cos\theta\left[\left(h_{rupt} - \sqrt{h_{rupt}^2+a^2}\right) - \left((h_{a,i}+h_{a,j}) - \sqrt{(h_{a,i}+h_{a,j})^2+a^2}\right)\right] \quad (99)$$

If we adopt the same thermodynamic analogy as that explained in the previous section, $L_{cap,app}$ and $L_{cap,sep}$ can be represented by:

$$L_{cap,app} = -W_{cap,app} = -2\pi\gamma_l r_{p,s,ij}\cos\theta\left[\left((h_{0,i}+h_{0,j}) - \sqrt{(h_{0,i}+h_{0,j})^2+a^2}\right) - \left((h_{a,i}+h_{a,j}) - \sqrt{(h_{a,i}+h_{a,j})^2+a^2}\right)\right] \quad (100)$$

$$L_{cap,sep} = -W_{cap,sep} = 2\pi\gamma_l r_{p,s,ij}\cos\theta\left[\left(h_{rupt} - \sqrt{h_{rupt}^2+a^2}\right) - \left((h_{a,i}+h_{a,j}) - \sqrt{(h_{a,i}+h_{a,j})^2+a^2}\right)\right] \quad (101)$$

These equations indicate that for a highly wetting system, the kinetic energies of colliding particles increase during the approach stage and decrease during the separation stage if solely considering the liquid bridge capillary effect. If the kinetic energies of colliding particles are such that both particles reach the solid-solid contact point, $L_{cap,app,i}$ and $L_{cap,app,j}$ can be defined as follows when considering the remarks mentioned in the previous section for the calculations of $L_{vis,app,i}$ and $L_{vis,app,j}$:

$$L_{cap,app,i} = \frac{v_{0,i}}{v_{0,i}+v_{0,j}}L_{cap,app} = \frac{v_{0,i}}{v_{0,i}+v_{0,j}}\left[-2\pi\gamma_l r_{p,s,ij}\cos\theta\left[\left((h_{0,i}+h_{0,j}) - \sqrt{(h_{0,i}+h_{0,j})^2+a^2}\right) - \left((h_{a,i}+h_{a,j}) - \sqrt{(h_{a,i}+h_{a,j})^2+a^2}\right)\right]\right] \quad (102)$$

$$L_{cap,app,j}=\frac{v_{0,j}}{v_{0,i}+v_{0,j}}L_{cap,app}=\frac{v_{0,j}}{v_{0,i}+v_{0,j}}\left[-2\pi\gamma_l r_{p,s,ij}\cos\theta\left[\left(\left(h_{0,i}+h_{0,j}\right)-\sqrt{\left(h_{0,i}+h_{0,j}\right)^2+a^2}\right)-\left(\left(h_{a,i}+h_{a,j}\right)-\sqrt{\left(h_{a,i}+h_{a,j}\right)^2+a^2}\right)\right]\right] \tag{103}$$

If particles i and j simultaneously stop prior to the solid-solid contact point, $L_{cap,app,i}$ and $L_{cap,app,j}$ can be respectively calculated by Eqs. (102) and (103), while replacing $(h_{a,i}+h_{a,j})$ by a relevant D in these equations. Considering the remarks mentioned in Section 2.3.1 for the calculations of $L_{vis,sep,i}$ and $L_{vis,sep,j}$, if both colliding wet particles can reach the liquid bridge rupture point, $L_{cap,sep,i}$ and $L_{cap,sep,j}$ can be given by:

$$L_{cap,sep,i}=\frac{\prime_{c,sep,i}}{\prime_{c,sep,i}+\prime_{c,sep,j}}L_{cap,sep}=\frac{\prime_{c,sep,i}}{\prime_{c,sep,i}+\prime_{c,sep,j}}\left[2\pi\gamma_l r_{p,s,ij}\cos\theta\left[\left(h_{rupt}-\sqrt{{h_{rupt}}^2+a^2}\right)-\left(\left(h_{a,i}+h_{a,j}\right)-\sqrt{\left(h_{a,i}+h_{a,j}\right)^2+a^2}\right)\right]\right] \tag{104}$$

$$L_{cap,sep,j}=\frac{\prime_{c,sep,j}}{\prime_{c,sep,i}+\prime_{c,sep,j}}L_{cap,sep}=\frac{\prime_{c,sep,j}}{\prime_{c,sep,i}+\prime_{c,sep,j}}\left[2\pi\gamma_l r_{p,s,ij}\cos\theta\left[\left(h_{rupt}-\sqrt{{h_{rupt}}^2+a^2}\right)-\left(\left(h_{a,i}+h_{a,j}\right)-\sqrt{\left(h_{a,i}+h_{a,j}\right)^2+a^2}\right)\right]\right] \tag{105}$$

If particles i and j simultaneously stop prior to the liquid bridge rupture point during the separation stage, we can calculate $L_{cap,sep,i}$ and $L_{cap,sep,j}$ with Eqs. (104) and (105), respectively, when replacing h_{rupt} by a relevant D in these equations.

2.3.3. Loss of energy due to the net effect of body forces

As noted in Section 2.2, the magnitudes of the body forces acting on colliding particles i and j could be different from each other when the particles differ in size and/or mass. The difference in the net of body forces acting on the colliding particles along the normal collision axis causes them to have different contributions on the outcome of the collision. In addition, the net effect of body forces on each colliding wet particle contributes differently on the collision outcome during the approach and separation stages. These points need to be properly taken into account in the calculations of losses of energy due to the net effect of body forces on the colliding particles and, hence, on the development of the generalized model. Accordingly, we consider the vector projections of the net of body forces acting on particles i and j along the corresponding unit vector $\vec{m}_{ij,app}$ or $\vec{m}_{ji,app}$ during the approach stage, or $\vec{m}_{ij,sep}$ or $\vec{m}_{ji,sep}$ during the separation stage. These unit vectors are defined based on the unit vector along the velocity of the target particle i relative to the colliding neighbor particle j along the normal collision axis $\vec{m}_{ij}$ and the unit vector along the velocity of particle j relative to particle i along the normal collision axis $\vec{m}_{ji}$, which are expressed as follows:

$$\vec{m}_{ij}=\frac{\vec{u}_{ij,\vec{n}_{ij}}}{\left|\vec{u}_{ij,\vec{n}_{ij}}\right|} \tag{106}$$

$$\vec{m}_{ji}=\frac{\vec{u}_{ji,\vec{n}_{ji}}}{\left|\vec{u}_{ji,\vec{n}_{ji}}\right|} \tag{107}$$

where $\vec{u}_{ij,\vec{n}_{ij}}$ is the velocity of particle i relative to particle j with respect to the reference frame I along $\vec{n}_{ij}$. $\vec{u}_{ji,\vec{n}_{ji}}$ is the velocity of particle j relative to particle i with respect to the reference frame I along $\vec{n}_{ji}$. $u_{ij,\vec{n}_{ij}}\geq 0$ during the approach stage and is equal to or less than zero during the separation stage. The same trends exist for the scalar projection of the velocity of particle j relative to particle i with respect to the reference frame I along $\vec{n}_{ji}$ ($u_{ji,\vec{n}_{ji}}$) during the approach and separation stages. Hence, $\vec{m}_{ij,app}$, $\vec{m}_{ji,app}$, $\vec{m}_{ij,sep}$, and $\vec{m}_{ji,sep}$ are defined as follows:

$$\vec{m}_{ij,app}=\vec{n}_{ij} \tag{108}$$

$$\vec{m}_{ji,app}=\vec{n}_{ji} \tag{109}$$

$$\vec{m}_{ij,sep}=-\vec{n}_{ij} \tag{110}$$

$$\vec{m}_{ji,sep}=-\vec{n}_{ji} \tag{111}$$

Schematic representations of forces acting on colliding wet particles during the approach and separation stages are illustrated in Fig. 4. In this figure, φ is the angle between a force and corresponding unit vector along the relative velocity between the colliding particles along the normal collision axis.

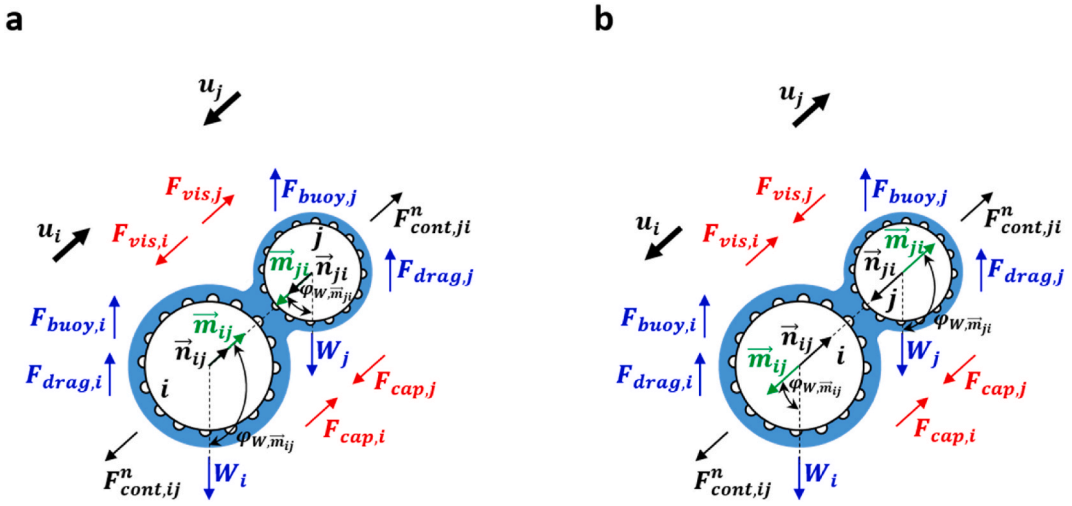

Fig. 4. Schematic representations of unit vectors along the normal collision axis and force distribution on colliding wet particles during the a) approach and b) separation stages.

Considering the assumption (xii) in Section 2.1, the fact that D decreases from $h_{0,i}+h_{0,j}$ to $h_{a,i}+h_{a,j}$ in the approach stage if both colliding wet particles have enough energy to reach the solid-solid contact point, and the remarks provided in Section 2.3.1 for the distance portion travelled by particles i and j during the approach stage, the total work done by the net effect of buoyant, drag, and gravity forces for particles i and j during the approach stage ($W_{bdw,app,i}$ and $W_{bdw,app,j}$, respectively) can be estimated as follows:

$$W_{bdw,app,i}=\int_{\frac{v_{0,j}}{v_{0,i}+v_{0,j}}\left(h_{0,i}+h_{0,j}\right)}^{\frac{v_{0,i}}{v_{0,i}+v_{0,j}}\left(h_{a,i}+h_{a,j}\right)}\overrightarrow{F}_{net,bdw,i,\overrightarrow{m}_{ij,app}}\bullet\left(\overrightarrow{e}_x\,dD_i\right)=F_{net,bdw,i,\overrightarrow{m}_{ij,app}}\frac{v_{0,i}}{v_{0,i}+v_{0,j}}\left[\left(h_{0,i}+h_{0,j}\right)-\left(h_{a,i}+h_{a,j}\right)\right] \tag{112}$$

$$W_{bdw,app,j}=\int_{\frac{v_{0,j}}{v_{0,i}+v_{0,j}}\left(h_{0,i}+h_{0,j}\right)}^{\frac{v_{0,j}}{v_{0,i}+v_{0,j}}\left(h_{a,i}+h_{a,j}\right)}\overrightarrow{F}_{net,bdw,j,\overrightarrow{m}_{ji,app}}\bullet\left(-\overrightarrow{e}_x\right)dD_j=F_{net,bdw,j,\overrightarrow{m}_{ji,app}}\frac{v_{0,j}}{v_{0,i}+v_{0,j}}\left[\left(h_{0,i}+h_{0,j}\right)-\left(h_{a,i}+h_{a,j}\right)\right] \tag{113}$$

where $\overrightarrow{F}_{net,bdw,i,\overrightarrow{m}_{ij,app}}$ and $\overrightarrow{F}_{net,bdw,j,\overrightarrow{m}_{ji,app}}$ are the vector projections of the net of body forces acting on particle i along $\overrightarrow{m}_{ij,app}$ and on particle j along $\overrightarrow{m}_{ji,app}$, respectively. D_i and D_j are the distances travelled by particles i and j, respectively. $\overrightarrow{F}_{net,bdw,i,\overrightarrow{m}_{ij,app}}$ and $\overrightarrow{F}_{net,bdw,j,\overrightarrow{m}_{ji,app}}$ can be calculated as follows:

$$\overrightarrow{F}_{net,bdw,i,\overrightarrow{m}_{ij,app}}=\frac{\left(\overrightarrow{F}_{net,bdw,i}\bullet\overrightarrow{m}_{ij,app}\right)}{\left|\overrightarrow{m}_{ij,app}\right|^2}\overrightarrow{m}_{ij,app} \tag{114}$$

$$\overrightarrow{F}_{net,bdw,j,\overrightarrow{m}_{ji,app}}=\frac{\left(\overrightarrow{F}_{net,bdw,j}\bullet\overrightarrow{m}_{ji,app}\right)}{\left|\overrightarrow{m}_{ji,app}\right|^2}\overrightarrow{m}_{ji,app} \tag{115}$$

where $\overrightarrow{F}_{net,bdw,i}$ and $\overrightarrow{F}_{net,bdw,j}$ are respectively the net vectors of body forces acting on particles i and j, which can be estimated as:

$$\overrightarrow{F}_{net,bdw,i}=\overrightarrow{F}_{buoy,i}+\overrightarrow{F}_{drag,i}+\overrightarrow{W}_i \tag{116}$$

$$\overrightarrow{F}_{net,bdw,j}=\overrightarrow{F}_{buoy,j}+\overrightarrow{F}_{drag,j}+\overrightarrow{W}_j \tag{117}$$

$F_{net,bdw,i,\overrightarrow{m}_{ij,app}}$ and $F_{net,bdw,j,\overrightarrow{m}_{ji,app}}$ can be expressed as follows:

$$F_{net,bdw,i,\overrightarrow{m}_{ij,app}}=\frac{\overrightarrow{F}_{net,bdw,i}\bullet\overrightarrow{m}_{ij,app}}{\left|\overrightarrow{m}_{ij,app}\right|} \tag{118}$$

$$F_{net,bdw,j,\overrightarrow{m}_{ji,app}} = \frac{\overrightarrow{F}_{net,bdw,j} \bullet \overrightarrow{m}_{ji,app}}{\left|\overrightarrow{m}_{ji,app}\right|} \tag{119}$$

We can calculate the total work done by the net effect of buoyant, drag, and gravity forces for particles i and j during the separation stage ($W_{bdw,sep,i}$ and $W_{bdw,sep,j}$, respectively) as follows:

$$W_{bdw,sep,i} = \int_{\frac{r_{c,sep,i}}{r_{c,sep,i}+r_{c,sep,j}}\left(h_{a,i}+h_{a,j}\right)}^{\frac{r_{c,sep,i}}{r_{c,sep,i}+r_{c,sep,j}}h_{rupt}} \overrightarrow{F}_{net,bdw,i,\overrightarrow{m}_{ij,sep}} \bullet \left(\overrightarrow{e}_x \, dD_i\right) = F_{net,bdw,i,\overrightarrow{m}_{ij,sep}} \frac{r_{c,sep,i}}{r_{c,sep,i}+r_{c,sep,j}} \left[h_{rupt} - \left(h_{a,i}+h_{a,j}\right)\right] \tag{120}$$

$$W_{bdw,sep,j} = \int_{\frac{r_{c,sep,j}}{r_{c,sep,i}+r_{c,sep,j}}\left(h_{a,i}+h_{a,j}\right)}^{\frac{r_{c,sep,j}}{r_{c,sep,i}+r_{c,sep,j}}h_{rupt}} \overrightarrow{F}_{net,bdw,j,\overrightarrow{m}_{ji,sep}} \bullet \left(-\overrightarrow{e}_x\right) dD_j = F_{net,bdw,j,\overrightarrow{m}_{ji,sep}} \frac{r_{c,sep,i}}{r_{c,sep,i}+r_{c,sep,j}} \left[h_{rupt} - \left(h_{a,i}+h_{a,j}\right)\right] \tag{121}$$

Eqs. (120) and (121) are obtained noting the assumption (xii) in Section 2.1, the fact that D increases from $h_{a,i}+h_{a,j}$ to h_{rupt} in the separation stage if both colliding wet particles have enough energy to reach the liquid bridge rupture point, and the remarks provided in Section 2.3.1 for the distance portion travelled by colliding particles i and j during the separation stage. In these equations, $\overrightarrow{F}_{net,bdw,i,\overrightarrow{m}_{ij,sep}}$ and $\overrightarrow{F}_{net,bdw,j,\overrightarrow{m}_{ji,sep}}$ are respectively the vector projections of the net of body forces acting on particle i along $\overrightarrow{m}_{ij,sep}$ and on particle j along $\overrightarrow{m}_{ji,sep}$. $\overrightarrow{F}_{net,bdw,i,\overrightarrow{m}_{ij,sep}}$, $\overrightarrow{F}_{net,bdw,j,\overrightarrow{m}_{ji,sep}}$, $F_{net,bdw,i,\overrightarrow{m}_{ij,sep}}$ and $F_{net,bdw,j,\overrightarrow{m}_{ji,sep}}$ can be estimated as follows:

$$\overrightarrow{F}_{net,bdw,i,\overrightarrow{m}_{ij,sep}} = \frac{\left(\overrightarrow{F}_{net,bdw,i} \bullet \overrightarrow{m}_{ij,sep}\right)}{\left|\overrightarrow{m}_{ij,sep}\right|^2} \overrightarrow{m}_{ij,sep} \tag{122}$$

$$\overrightarrow{F}_{net,bdw,j,\overrightarrow{m}_{ji,app}} = \frac{\left(\overrightarrow{F}_{net,bdw,j} \bullet \overrightarrow{m}_{ji,sep}\right)}{\left|\overrightarrow{m}_{ji,sep}\right|^2} \overrightarrow{m}_{ji,sep} \tag{123}$$

$$F_{net,bdw,i,\overrightarrow{m}_{ij,sep}} = \frac{\overrightarrow{F}_{net,bdw,i} \bullet \overrightarrow{m}_{ij,sep}}{\left|\overrightarrow{m}_{ij,sep}\right|} \tag{124}$$

$$F_{net,bdw,j,\overrightarrow{m}_{ji,sep}} = \frac{\overrightarrow{F}_{net,bdw,j} \bullet \overrightarrow{m}_{ji,sep}}{\left|\overrightarrow{m}_{ji,sep}\right|} \tag{125}$$

Adopting the thermodynamic analogy explained in Section 2.3.1, $L_{bdw,app,i}$, $L_{bdw,app,j}$, $L_{bdw,sep,i}$, and $L_{bdw,sep,j}$ can be given by:

$$L_{bdw,app,i} = -W_{bdw,app,i} = -F_{net,bdw,i,\overrightarrow{m}_{ij,app}} \frac{v_{0,i}}{v_{0,i}+v_{0,j}} \left[\left(h_{0,i}+h_{0,j}\right) - \left(h_{a,i}+h_{a,j}\right)\right] \tag{126}$$

$$L_{bdw,app,j} = -W_{bdw,app,j} = -F_{net,bdw,j,\overrightarrow{m}_{ji,app}} \frac{v_{0,j}}{v_{0,i}+v_{0,j}} \left[\left(h_{0,i}+h_{0,j}\right) - \left(h_{a,i}+h_{a,j}\right)\right] \tag{127}$$

$$L_{bdw,sep,i} = -W_{bdw,sep,i} = -F_{net,bdw,i,\overrightarrow{m}_{ij,sep}} \frac{r_{c,sep,i}}{r_{c,sep,i}+r_{c,sep,j}} \left[h_{rupt} - \left(h_{a,i}+h_{a,j}\right)\right] \tag{128}$$

$$L_{bdw,sep,j} = -W_{bdw,sep,j} = -F_{net,bdw,j,\overrightarrow{m}_{ji,sep}} \frac{r_{c,sep,i}}{r_{c,sep,i}+r_{c,sep,j}} \left[h_{rupt} - \left(h_{a,i}+h_{a,j}\right)\right] \tag{129}$$

2.3.4. Solid-solid contact loss

According to Gidaspow [47], the following correlation can be employed to calculate the total contact loss for a dry inelastic collision between two particles $L_{c,tot}$:

$$L_{c,tot} = \frac{1}{2} \frac{m_{p,i} m_{p,j}}{m_{p,i}+m_{p,j}} \left(1-e^2\right) \left(\overrightarrow{n}_{ij} \bullet \overrightarrow{u}_{c,rel}\right)^2 \tag{130}$$

where $\overrightarrow{u}_{c,rel}$ is the relative contact velocity between the colliding particles with respect to the reference frame I. Since in the algorithm presented in Fig. 3 for the generalized model we monitor the kinetic energy of each particle during the collision interval, we need to have an estimate of the contribution of each particle in the solid-solid contact loss. This cannot easily be obtained with Eq. (130). Based on the assumption (xvi) in Section 2.1, the net of external forces can be neglected at the solid-solid contact point. Thus, the

conservation of momentum, as presented below, can be applied under that condition.

$$m_{p,i}\overrightarrow{\nu}_{c,app,i} + m_{p,j}\overrightarrow{\nu}_{c,app,j} = m_{p,i}\overrightarrow{\nu}_{c,sep,i} + m_{p,j}\overrightarrow{\nu}_{c,sep,j} \tag{131}$$

Consequently, the following formula that represents the kinetic energy change during a collision, becomes a formula for the loss of kinetic energy when no external forces are acting on the colliding particles at the solid-solid contact point:

$$L_{c,tot} = \frac{1}{2}m_{p,i}\left(\nu_{c,app,i}^{\ 2} - \nu_{c,sep,i}^{\ 2}\right) + \frac{1}{2}m_{p,j}\left(\nu_{c,app,j}^{\ 2} - \nu_{c,sep,j}^{\ 2}\right) \tag{132}$$

$L_{c,i}$ and $L_{c,j}$ can hence be calculated as follows:

$$L_{c,i} = \frac{1}{2}m_{p,i}\left(\nu_{c,app,i}^{\ 2} - \nu_{c,sep,i}^{\ 2}\right) \tag{133}$$

$$L_{c,j} = \frac{1}{2}m_{p,j}\left(\nu_{c,app,j}^{\ 2} - \nu_{c,sep,j}^{\ 2}\right) \tag{134}$$

$\nu_{c,sep,i}$ and $\nu_{c,sep,j}$ can be estimated with the help of Eqs. (52) and (53), which themselves were obtained based on Eq. (131), and the following formula for e:

$$e = \frac{\overrightarrow{\nu}_{c,sep,j} - \overrightarrow{\nu}_{c,sep,i}}{\overrightarrow{\nu}_{c,app,i} - \overrightarrow{\nu}_{c,app,j}} \tag{135}$$

2.3.5. Special cases during the approach and separation stages

During either the approach or separation stage of a binary collision of wet particles, some special conditions may be experienced, where one particle stops moving while the other one can still continue its movement. We handled these cases in the proposed generalized model with the help of some kinetic energy parameters (refer to Fig. 3). For instance, if the target particle i loses all its initial kinetic energy during the approach stage before reaching the solid-solid contact point, while the colliding neighbor particle j has some energy to approach particle i, we need to first determine $D_{app,i}$. This can be achieved by solving (or finding the global minimum of) the following nonlinear function of D:

$$1 - \left(L_{cap,mid,app,i} + L_{vis,mid,app,i} + L_{bdw,mid,app,i}\right) / K_{ini,i} = 0 \tag{136}$$

where $L_{cap,mid,app,i}$, $L_{vis,mid,app,i}$, and $L_{bdw,mid,app,i}$ are respectively the losses of energy due to the capillary and viscous effects, as well as the net effect of body forces for particle i in the distance interval of $(h_{0,i} + h_{0,j})$ to $D_{app,i}$ during the approach stage. $K_{ini,i}$ is estimated by Eq. (34), while $L_{cap,mid,app,i}$, $L_{vis,mid,app,i}$, and $L_{bdw,mid,app,i}$ are calculated as follows:

$$L_{cap,mid,app,i} = \frac{v_{0,i}}{v_{0,i}+v_{0,j}}\left[L_{cap,app}\Big|_{h_{0,i}+h_{0,j}}^{D_{app,i}}\right] = \frac{v_{0,i}}{v_{0,i}+v_{0,j}}\left[-2\pi\gamma_l r_{p,s,ij}\cos\theta\left[\left(\left(h_{0,i}+h_{0,j}\right) - \sqrt{\left(h_{0,i}+h_{0,j}\right)^2 + a^2}\right) - \left(D_{app,i} - \sqrt{D_{app,i}^{\ 2} + a^2}\right)\right]\right] \tag{137}$$

$$L_{vis,mid,app,i} = \frac{v_{0,i}}{v_{0,i}+v_{0,j}}\left[L_{vis,app}\Big|_{h_{0,i}+h_{0,j}}^{D_{app,i}}\right] = \frac{v_{0,i}}{v_{0,i}+v_{0,j}}\left[\left(A_i+A_j\right)\ln\left(\frac{f\left(h_{0,i}+h_{0,j}\right)}{f\left(D_{app,i}\right)}\right) + \left(\frac{A_i}{2St_{v,i}} + \frac{A_j}{2St_{v,j}}\right)\left[ln^2\left(f\left(h_{0,i}+h_{0,j}\right)\right) - ln^2\left(f\left(D_{app,i}\right)\right) - 2\ln\left(f\left(h_{0,i}+h_{0,j}\right)\right)\ln\left(\frac{f\left(h_{0,i}+h_{0,j}\right)}{f\left(D_{app,i}\right)}\right)\right]\right] \tag{138}$$

$$L_{bdw,mid,app,i} = -W_{bdw,app,i}\Big|_{\frac{v_{0,i}}{v_{0,i}+v_{0,j}}\left(h_{0,i}+h_{0,j}\right)}^{\frac{v_{0,i}}{v_{0,i}+v_{0,j}}D_{app,i}} = -F_{net,bdw,i,\overrightarrow{m}_{ij,app}}\frac{v_{0,i}}{v_{0,i}+v_{0,j}}\left[\left(h_{0,i}+h_{0,j}\right) - D_{app,i}\right] \tag{139}$$

We, subsequently, estimate $\mathbb{K}_{mid,app,j}$ based on Eq. (39). For this estimation, $\mathbb{L}_{cap,app,j}$, $L_{vis,mid,app,j-i}$, and $\mathbb{L}_{bdw,app,j}$ are given by:

$$\mathbb{L}_{cap,app,j} = \frac{v_{0,j}}{v_{0,i}+v_{0,j}}\left[L_{cap,app}\Big|_{h_{0,i}+h_{0,j}}^{D_{app,i}}\right] + L_{cap,app}\Big|_{D_{app,i}}^{h_{a,i}+h_{a,j}} = \frac{v_{0,j}}{v_{0,i}+v_{0,j}}\left[-2\pi\gamma_l r_{p,s,ij}\cos\theta\left[\left(\left(h_{0,i}+h_{0,j}\right) - \sqrt{\left(h_{0,i}+h_{0,j}\right)^2+a^2}\right) - \left(D_{app,i} - \sqrt{D_{app,i}^{\ 2}+a^2}\right)\right]\right] + \left[-2\pi\gamma_l r_{p,s,ij}\cos\theta\left[\left(D_{app,i} - \sqrt{D_{app,i}^{\ 2}+a^2}\right) - \left(\left(h_{a,i}+h_{a,j}\right) - \sqrt{\left(h_{a,i}+h_{a,j}\right)^2+a^2}\right)\right]\right] \tag{140}$$

$$L_{vis,mid,app,j-i} = \frac{v_{0,j}}{v_{0,i}+v_{0,j}}\left[L_{vis,app}\Big|_{h_{0,i}+h_{0,j}}^{D_{app,i}}\right] = \frac{v_{0,j}}{v_{0,i}+v_{0,j}}\left[\left(A_i+A_j\right)\ln\left(\frac{f\left(h_{0,i}+h_{0,j}\right)}{f\left(D_{app,i}\right)}\right) + \left(\frac{A_i}{2St_{v,i}} + \frac{A_j}{2St_{v,j}}\right)\left[ln^2\left(f\left(h_{0,i}+h_{0,j}\right)\right) - ln^2\left(f\left(D_{app,i}\right)\right) - 2\ln\left(f\left(h_{0,i}+h_{0,j}\right)\right)\ln\left(\frac{f\left(h_{0,i}+h_{0,j}\right)}{f\left(D_{app,i}\right)}\right)\right]\right] \tag{141}$$

$$\mathbb{L}_{bdw,app,j} = \left(-W_{bdw,app,j}\Big|_{\frac{v_{0,j}}{v_{0,i}+v_{0,j}}D_{app,i}}^{\frac{v_{0,j}}{v_{0,i}+v_{0,j}}\left(h_{0,i}+h_{0,j}\right)} \right) + \left(-W_{bdw,app,j}\Big|_{D_{app,i}}^{h_{a,i}+h_{a,j}} \right) = -F_{net,bdw,j,\overrightarrow{m}_{ji,app}} \frac{v_{0,j}}{v_{0,j}+v_{0,j}} \left[\left(h_{0,i}+h_{0,j}\right) - D_{app,i} \right]$$
$$- F_{net,bdw,j,\overrightarrow{m}_{ji,app}} \left[D_{app,i} - \left(h_{a,i}+h_{a,j}\right) \right] \quad (142)$$

To calculate $\mathbb{L}_{cap,app,j}$ and $\mathbb{L}_{bdw,app,j}$, we considered that both colliding particles move by $D_{app,i}$, while particle j may solely continue the approach stage in the distance interval of $D_{app,i}$ to $(h_{a,i}+h_{a,j})$. Including the losses of energy in the distance interval of $D_{app,i}$ to $(h_{a,i}+h_{a,j})$ during the approach stage in Eqs. (140) and (142) avoids repetition of collision outcome verification steps. This is owing to the facts that (i) in a highly wetting system, the capillary effect increases the kinetic energy of a colliding particle during the approach stage, (ii) the viscous effect always dissipates the kinetic energy of the particle, (iii) the net effect of body forces during the approach stage may increase, decrease or have no influence on the kinetic energy of the particle, and (iv) we employ the superposition principle in the analytical energy balance model to estimate the total loss of energy by the particle. The colliding wet particles agglomerate if $\mathbb{K}_{mid,app,j} \leq 0$ since the net of all losses of energy in the distance interval of $(h_{0,i}+h_{0,j})$ to $D_{app,i}$ and losses of energy due to the capillary effect and the net effect of body forces in the distance interval of $D_{app,i}$ to $(h_{a,i}+h_{a,j})$ yield an insufficient kinetic energy for particle j to further approach to the target particle, while the viscous effect in the distance interval of $D_{app,i}$ to $(h_{a,i}+h_{a,j})$ can additionally prevent its movement. Otherwise, we need to check whether the viscous loss of energy for particle j can completely dissipate $\mathbb{K}_{mid,app,j}$ in the distance interval of $D_{app,i}$ to $(h_{a,i}+h_{a,j})$ during the approach stage. This can be verified by monitoring $\mathbb{v}_{c,app,vis,j}$. As demonstrated in Section S-9 of the Supplementary Material, particles will form an agglomerate if $\mathbb{v}_{c,app,vis,j} \leq 0$, while calculations for the evaluation of the collision outcome will otherwise be continued. We can obtain expressions for the approach speed of particle j with respect to the CM of the colliding particles during the approach stage (based on $\mathbb{v}_{mid,app,j}$) for $\mathbb{v}_{app,vis,j}$ and $\mathbb{v}_{c,app,vis,j}$ by repeating the same procedure as what was described in Section 2.3.1 when substituting Eq. (S.9a) into Eq. (S.1a) and noting the initial particle speed of $\mathbb{v}_{mid,app,j}$ at $D_{app,i}$. Hence, $\mathbb{v}_{app,vis,j}$ and $\mathbb{v}_{c,app,vis,j}$ can be expressed as follows (see Section S-8 of the Supplementary Material for details):

$$\mathbb{v}_{app,vis,j} = \begin{cases} \frac{v_{0,j}}{St_{v,j}} \left(\frac{\mathbb{v}_{mid,app,j} St_{v,j}}{v_{0,j}} - \ln\left(\frac{f\left(D_{app,i}\right)}{f(D)} \right) \right), & St_{v,j} > \frac{v_{0,j}}{\mathbb{v}_{mid,app,j}} \ln\left(\frac{f\left(D_{app,i}\right)}{f(D)} \right) \\ 0, & St_{v,j} \leq \frac{v_{0,j}}{\mathbb{v}_{mid,app,j}} \ln\left(\frac{f\left(D_{app,i}\right)}{f(D)} \right) \end{cases} \quad (143)$$

$$\mathbb{v}_{c,app,vis,j} = \begin{cases} \frac{v_{0,j}}{St_{v,j}} \left(\frac{\mathbb{v}_{mid,app,j} St_{v,j}}{v_{0,j}} - \ln\left(\frac{f\left(D_{app,i}\right)}{f\left(h_{a,i}+h_{a,j}\right)} \right) \right), & St_{v,j} > \frac{v_{0,j}}{\mathbb{v}_{mid,app,j}} \ln\left(\frac{f\left(D_{app,i}\right)}{f\left(h_{a,i}+h_{a,j}\right)} \right) \\ 0, & St_{v,j} \leq \frac{v_{0,j}}{\mathbb{v}_{mid,app,j}} \ln\left(\frac{f\left(D_{app,i}\right)}{f\left(h_{a,i}+h_{a,j}\right)} \right) \end{cases} \quad (144)$$

With a similar approach to what was explained in Section 2.3.1, we can estimate $\mathbb{L}_{vis,app,j}$ as follows when employing Eq. (S.9a) with Eq. (143) (see Section S-8 of the Supplementary Material for details):

$$\mathbb{L}_{vis,app,j} = -\int_{D_{app,i}}^{h_{a,i}+h_{a,j}} \overrightarrow{F}_{vis,j} \bullet \left(-\overrightarrow{e}_x \right) dD = \frac{A_j \mathbb{v}_{mid,app,j}}{v_{0,j}} \ln\left(\frac{f\left(D_{app,i}\right)}{f\left(h_{a,i}+h_{a,j}\right)} \right) + \frac{A_j}{2St_{v,j}} \left[ln^2\left(f\left(D_{app,i}\right)\right) - ln^2\left(f\left(h_{a,i}+h_{a,j}\right)\right) \right.$$
$$\left. - 2\ln\left(f\left(D_{app,i}\right)\right) \ln\left(\frac{f\left(D_{app,i}\right)}{f\left(h_{a,i}+h_{a,j}\right)} \right) \right] \quad (145)$$

We followed the same procedure as what was described in this section for other special cases, i.e., when particle j loses all its initial kinetic energy during the approach stage before reaching the solid-solid contact point, while particle i has some energy to approach the colliding neighbor particle, or when one of the colliding particles stops during the separation stage, while the other particle can continue toward the liquid bridge rupture point. Please refer to Sections S-10 and S-12 of the Supplementary Material for details.

3. Results and discussion

3.1. Model verification

In this section, predictions with the generalized agglomeration model are compared with those from the non-generalized agglomeration model developed recently by the same authors for collisions involving identical wet particles [31]. As the contributions of body forces were neglected in the development of the non-generalized agglomeration model, the effect of collision direction on the outcome of a binary collision of wet particles could not be studied by this model. For this comparison, we assume that wet particles are identical and colliding with a collision angle $\beta = 0^\circ$ (refer to Fig. 5). In addition, for the comparison conducted in this section and analyses accomplished in the next sections, we postulate that colliding particles have identical impact speeds with respect to the reference frame I, the center of the target particle i is located at the origin of the frame I at the impact condition, and the collision happens at most in two dimensions, i.e., Y-Z plane as depicted in Fig. 5. These assumptions help more conveniently define the particle

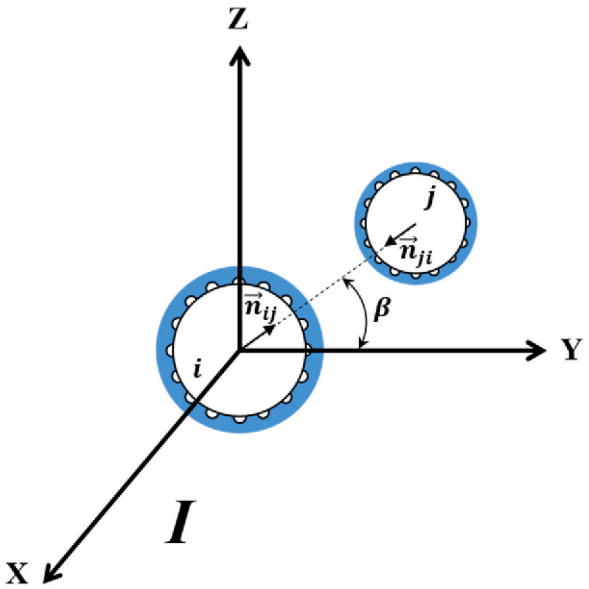

Fig. 5. Schematic representation of a two-dimensional collision of two non-identical wet particles. Remark: gravity acts in the Z direction.

positions at the impact condition based on their dimension, coating layer thickness, and collision angle information, and analyze the results based on the critical impact speed u_0^*, defined here as the minimum $u_{0,i,\vec{n}_{ij}}$ required for the particles to rebound. For simplicity, unless otherwise specified, we represent $u_{0,i,\vec{n}_{ij}}$ by u_0 in the results and discussions to be presented in this study.

We conducted the comparison for two liquid coatings: the first being water at ambient conditions representing a low viscosity liquid, and the second being a high viscosity liquid with typical slag properties. These cases may be applicable to granulation [22,50] and fluidized bed gasification or combustion [5,51] processes, respectively. For these reference cases, it has been assumed that coarse silica sand forms the base particle, particles are colliding in the emulsion phase of a gas-solid fluidized bed, and air is the fluidizing agent. In a gas-solid fluidized bed, the interstitial gas flow rate can be in excess of the minimum fluidization condition and the emulsion phase voidage can be greater than the minimum fluidization voidage [52–56]. Hence, for the calculations performed in this work, we assume that the superficial gas velocity of the emulsion phase $\vec{U}_e$ is 1.1 times the minimum fluidization velocity $\vec{U}_{mf}$, when dealing with identical wet particles, or 1.1 times the larger $\vec{U}_{mf}$, when non-identical wet particles are colliding. In this study, we adopted the correlation by Wen and Yu [57] to estimate the minimum fluidization speed U_{mf} of particles. The input parameters for the reference

Table 2
Input parameters to evaluate the performances of the non-generalized and generalized agglomeration models for two reference cases.

	Case I: water	Case II: hypothetical slag
Diameter of the target solid particle i, $d_{p,s,i}$ (μm)	1000	1000
Diameter of the colliding neighbor solid particle j, $d_{p,s,j}$ (μm)	1000	1000
Density of the target solid particle i, $\rho_{p,s,i}$ (kg/m^3)	2650	2650
Density of the colliding neighbor solid particle j, $\rho_{p,s,j}$ (kg/m^3)	2650	2650
Dry restitution coefficient, e (-)	0.90 [58]	0.90 [58]
Height of asperity on the surface of the target particle i, $h_{a,i}$ (μm)	0.10	0.10
Height of asperity on the surface of the colliding neighbor particle j, $h_{a,j}$ (μm)	0.10	0.10
Thickness of the coating layer on the surface of the target particle i, $h_{0,i}$ (μm)	5.00	0.15
Thickness of the coating layer on the surface of the colliding neighbor particle j, $h_{0,j}$ (μm)	5.00	0.15
Collision angle, β (deg)	0	0
Liquid viscosity, μ_l (Pa.s)	8.9×10^{-4}	10.0
Surface tension, γ_l (N/m)	0.073	0.400
Contact angle, θ (deg)	10	10
Liquid density, ρ_l (kg/m^3)	997	2500
Fluidizing agent (-)	Air	Air
Operating temperature, T (°C)	25	800
Operating pressure, P (bar)	1	1
Gas viscosity, μ_g (Pa.s)	18.48×10^{-6}	45.48×10^{-6}
Gas density, ρ_g (kg/m^3)	1.168	0.324
Superficial gas velocity of emulsion phase, $\vec{U}_e$ (m/s)	1.1 [0, 0, U_{mf}]	1.1 [0, 0, U_{mf}]
Local bed voidage, ε (-)	0.55	0.55

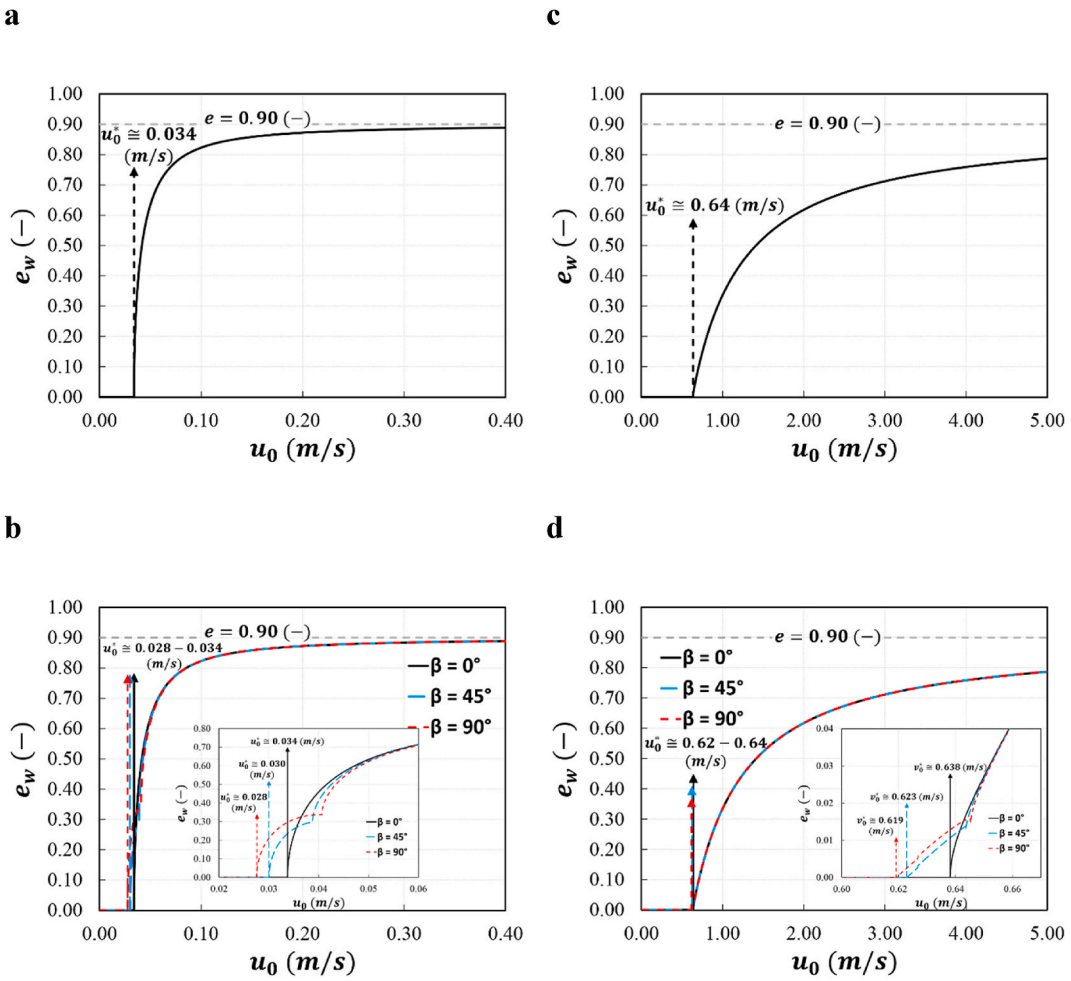

Fig. 6. Comparison of performances of the non-generalized and generalized agglomeration models for two reference cases. a) non-generalized model for water, b) generalized model for water, c) non-generalized model for slag, and d) generalized model for slag. Conditions are presented in Table 2.

cases are presented in Table 2.

The results of the non-generalized and generalized agglomeration models are illustrated in Fig. 6. In Figs. 6b and d, we included the results of collision angles other than zero, which will be discussed in Section 3.3. When water, a low viscosity liquid, acts as the liquid binder between particles, both non-generalized and generalized agglomeration models demonstrate identical and reasonable outcomes when $\beta = 0°$ (Figs. 6a and b). In other words, $e_w = 0$ at $u_0 \leq u_0^*$, it increases with the impact speed at $u_0 > u_0^*$, and reaches a plateau at $e_w \cong e = 0.90$ when $u_0 \geq 0.30$ m/s. Likewise, Figs. 6c and d shows that both the non-generalized and generalized agglomeration models exhibit identical trends when the liquid coating is a high viscosity slag and $\beta = 0°$. The results presented in Figs. 6c and d are also in broad agreement with the expectations. In particular, $e_w = 0$ at $u_0 \leq u_0^*$, and it gradually grows with the impact speed at $u_0 > u_0^*$ toward the dry restitution coefficient. Pairwise comparisons between Figs. 6a and c (results of the non-generalized agglomeration model), and Figs. 6b and d (results of the generalized agglomeration model), indicate that the presence of a coating layer of a high viscosity liquid on the surfaces of colliding particles can appreciably increase u_0^* compared to when wet particles are coated with a considerably thicker layer of a low viscosity liquid, 0.638 m/s vs. 0.034 m/s, respectively. Evaluating the capillary number for the reference cases, i.e., water and hypothetical slag as the liquid layer, at the corresponding u_0^* (8.3e-4 and 31.9, respectively) indicates that the system operates under capillary and viscous limiting conditions, respectively [59]. Therefore, for a binary collision of identical wet particles with $\beta = 0°$, the generalized agglomeration model can provide reasonable outcomes that are identical to those obtained from the non-generalized agglomeration model under both capillary and viscous limiting conditions with highly wetting systems. This can be regarded as the verification of the generalized model. It is also worth mentioning that all the viscous energy loss equations adopted in the evaluation algorithm of the generalized agglomeration model (Fig. 3) provide positive values, which are in accordance with the expectations as the viscous effect is always dissipative. Correcting the viscous energy loss equations of the original energy balance agglomeration model proposed by Darabi et al. [2] was one of the achievements that we made in our earlier study [31] and the

same mathematical treatment was implemented in the development of the generalized model in this study. This helps the generalized model provide reliable outcomes under both capillary and viscous limiting conditions with highly wetting systems.

3.2. Model validation

It would be ideal to validate the generalized model with experimental data for collision outcomes of non-identical wet particles covering both capillary and viscous limiting conditions. However, this is rare in literature. We, hence, adopted experimental data for wet collisions between a 1.74 mm glass particle and a plate at different layer thicknesses of water reported in the study by Buck et al. [12] for this purpose. Readers are referred to the work by Buck et al. [12] for experimental details. Results of comparison of predictions obtained by the generalized model and the corresponding experimental data are presented in Fig. 7. The model could successfully predict the experimental results, in particular, for thinner liquid layers. Like experimental results, the model predicts $e_w = 0$ (agglomeration conditions) at $u_0 \leq u_0^*$ and the e_w features a rapid increase at $u_0 > u_0^*$ to reach a plateau near e at high impact speeds. This can be interpreted as the validation of the generalized model. Note that the adopted liquid thicknesses in the experiments are considerably higher than what can be experienced in practice for particle agglomeration. The slight discrepancy between the model predictions and experimental data can be attributed to the adopted empirical correlations for estimations of viscous and capillary forces, as well as liquid bridge volume, and the potential deviation from the mentioned assumptions in Section 2.1 for the thick liquid layer scenarios experienced in experiment.

3.3. Effects of collision direction and some particle and liquid properties on collision outcome

Since the contributions of body forces on the outcome of a binary collision of wet particles were taken into account in the development of the generalized agglomeration model, we can delineate the influence of collision direction ($\beta = 0^\circ$ as the reference scenario in Fig. 5) on the collision outcome with this model. Since studying the collision angles between 0 and 90° clarifies all corresponding scenarios that may happen at collision angles between 0 and 360°, we focused on the first quarter range here. The results presented in Figs. 6b and d indicate that, for both reference cases studied here, the collision outcome and value of e_w can vary with the collision angle solely in a short range of impact speeds around u_0^*. In addition, we can have the following observations: (i) the greatest difference exists between e_w vs. u_0 profiles of $\beta = 0^\circ$ and 90°, corresponding to the horizontal and vertical collision scenarios with the minimum and maximum contributions of the body forces on the collision outcome, respectively, (ii) for collision angles other than zero (45° and 90°, here), e_w does not initially increase monotonously with u_0 at $u_0 > u_0^*$, which mainly reflects the special operational ranges, where one particle stops during either the approach or separation stage, while the other one continues to move, (iii) the relative effect of collision angle on e_w was more pronounced for the reference case I with water as the liquid layer.

Scrutinizing the estimated parameters during the calculation procedure reveals that at impact speeds close to u_0^*, the magnitude of net body forces approaches the magnitudes of liquid bridge-induced interparticle forces. Accordingly, at impact speeds close to u_0^*, the body forces could have an impact on the collision outcome and/or value of e_w, which is highlighted by the effect of collision angle on these items. Upon increasing the impact speed at $u_0 > u_0^*$ and deviating enough from u_0^*, the magnitude of the viscous force increases (the magnitude of the capillary force is insensitive to impact speed), leading to a decrease of the relative importance of body forces to interparticle forces. Hence, no sensible effect of body forces or collision direction on the collision outcome or e_w can be observed. Owing to a higher liquid viscosity and a greater relative speed between the colliding particles at $u_0 \geq u_0^*$ of the reference case II in comparison with the reference case I, the magnitude of viscous force for the reference case II is higher and increases more rapidly with u_0. These lead the contributions of body forces on the collision outcome to be less highlighted when particles are coated with a high

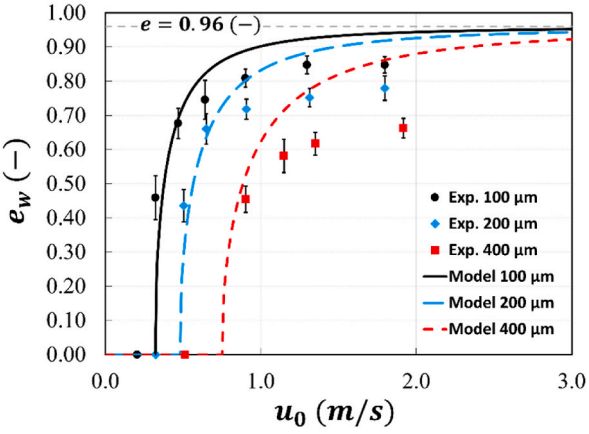

Fig. 7. Validation of the generalized agglomeration model with experimental data from Buck et al. [12] for wet collisions between a 1.74 mm glass particle and a plate at different layer thicknesses of water.

viscosity liquid. Hence, varying the collision angle for the reference case II has a limited relative influence on e_w, observed at very small values of e_w near u_0^*. The results discussed here indicate that if a processing unit operates with wet particles that are colliding at impact speeds close to the corresponding u_0^*, it is critical to include the contributions of body forces for the evaluation of collision outcomes. However, if impact speeds of colliding wet particles deviate enough from the corresponding u_0^*, the net of body forces has a minimal effect on the collision outcome.

In the next step, for the reference cases specified in Table 2, we simultaneously altered the collision angle and either the solid particle size or density, asperity heights or the thickness of liquid coating layers to investigate the effects of these parameters on the outcome of a binary collision of wet particles. For this analysis, a list of changes in some input parameters of the reference cases are reported in Table 3. The results of this analysis for water and slag coatings are presented in Figs. 8 and 9, respectively. In all scenarios investigated here, the collision angle can affect the collision outcome and value of e_w in a short range of impact speeds around u_0^*, as discussed above for Figs. 6b and d. Comparing Figs. 6b and 8a indicates that decreasing the size of one of the colliding particles slightly increases the span of u_0 over which the collision angle influences the collision outcome. It also increases u_0^*, which is analogous to an increase in the agglomeration tendency, for all collision angles. This trend can be attributed to the lower inertia of a smaller particle. This result suggests that a fluidized bed made of particles with a narrow size distribution can exhibit a lower agglomeration tendency than a bed having a wide particle size distribution, which is in broad agreement with experimental observations reported in literature [60]. Similar observations that are more pronounced than those observed in Figs. 6b and 8a can be obtained by comparing Figs. 6d and 9a when wet particles are coated with slag as the liquid layer.

Comparing Figs. 6b and 8b reveals that increasing the solid particle density of one of the colliding particles, from a typical density of silica sand to the density of an ilmenite ore particle, decreases u_0^* for all collision angles. We can have a similar observation when comparing Figs. 6d and 9b, although the effect is more pronounced. This dependency can be attributed to the higher inertia of a denser particle that increases the net inertia of colliding particles. This result recommends that a fluidized bed of mixed silica sand and ilmenite particles, which has been employed for the oxygen carrier aided combustion process [33,34], can show a lower agglomeration tendency than a bed merely comprised of silica sand particles at similar operating conditions and when both beds are adequately fluidized. Structural and chemical changes that ilmenite particles can experience during combustion of problematic fuels [61], e.g., biomass with a high potassium content, substantially decreases the formation of high viscosity liquid on the surface of particles. Integrating this feature with the findings obtained from Figs. 6d and 9b indicate that the simultaneous application of ilmenite and silica sand particles in a fluidized bed combustor can help improve the bed material agglomeration resistance. Experimental findings indicated that considerably lower and smaller agglomerates were observed in a bubbling fluidized bed combustor of coal blended with wheat straw pellets when ilmenite was adopted as the bed material compared to silica sand [62].

For the next scenarios, we investigated the effects of distribution and sum of asperity heights on the collision outcomes. No change is observed in e_w vs. u_0 profiles of water and slag coatings when we vary the values of asperity heights adopted for the reference cases, while keeping the sum of asperity heights constant (compare Figs. 6b and S.2a and Figs. 6d and S.3a for the water and slag cases, respectively). However, when $h_{a,i}$ and $h_{a,j}$ are simultaneously decreased from 0.10 μm to 0.08 μm, no change is observed for the e_w vs. u_0 profile of water coatings (Fig. 6b vs. Fig. 8c), while u_0^* considerably increases for all collision angles when particles are coated with slag (Fig. 6d vs. Fig. 9c). As addressed in Section 3.1, the reference cases with water and slag coatings operate under capillary and viscous limiting conditions, respectively. The observations made here reveals that the sum of asperity heights has a minimal influence on the collision outcome under capillary limiting conditions, while it has a considerable impact under viscous limiting conditions. This is in accordance with the expectations and results reported by Shabanian et al. [31], as the magnitude of the capillary force is independent of the asperity height and the loss of energy due to the capillary effect can be minimally affected by the sum of asperity heights. However, it has a significant influence on the magnitude of viscous force and the corresponding loss of kinetic energy. Two phenomena can mainly explain the increase in u_0^* with a decrease in the sum of asperity heights for a binary collision of particles coated with high viscosity slag: (i) decreasing D at very small separation distances between the colliding particles near the surface asperity size significantly increases the magnitude of viscous force and (ii) at constant thickness of liquid layers, decreasing the sum of asperity

Table 3
List of changes in some input parameters of the reference cases, presented in Table 2, to study the combined effects of collision angle and some particle and liquid properties on collision outcomes.

Change in	Solid particle size	Solid particle density	Height of a surface asperity		Thickness of coating layer			
	Cases I & II	Cases I & II	Cases I & II		Case I		Case II	
			A	B	A	B	A	B
$d_{p,s,i}$ (μm)	1000							
$d_{p,s,j}$ (μm)	600							
$\rho_{p,s,i}$ (kg/m^3)		2650						
$\rho_{p,s,j}$ (kg/m^3)		4330						
$h_{a,i}$ (μm)			0.08	0.08				
$h_{a,j}$ (μm)			0.12	0.08				
$h_{0,i}$ (μm)					3.00	7.50	0.12	0.20
$h_{0,j}$ (μm)					7.00	7.50	0.18	0.20
β (deg)	0, 90, 270	0, 90, 270	0, 45, 90		0, 45, 90			

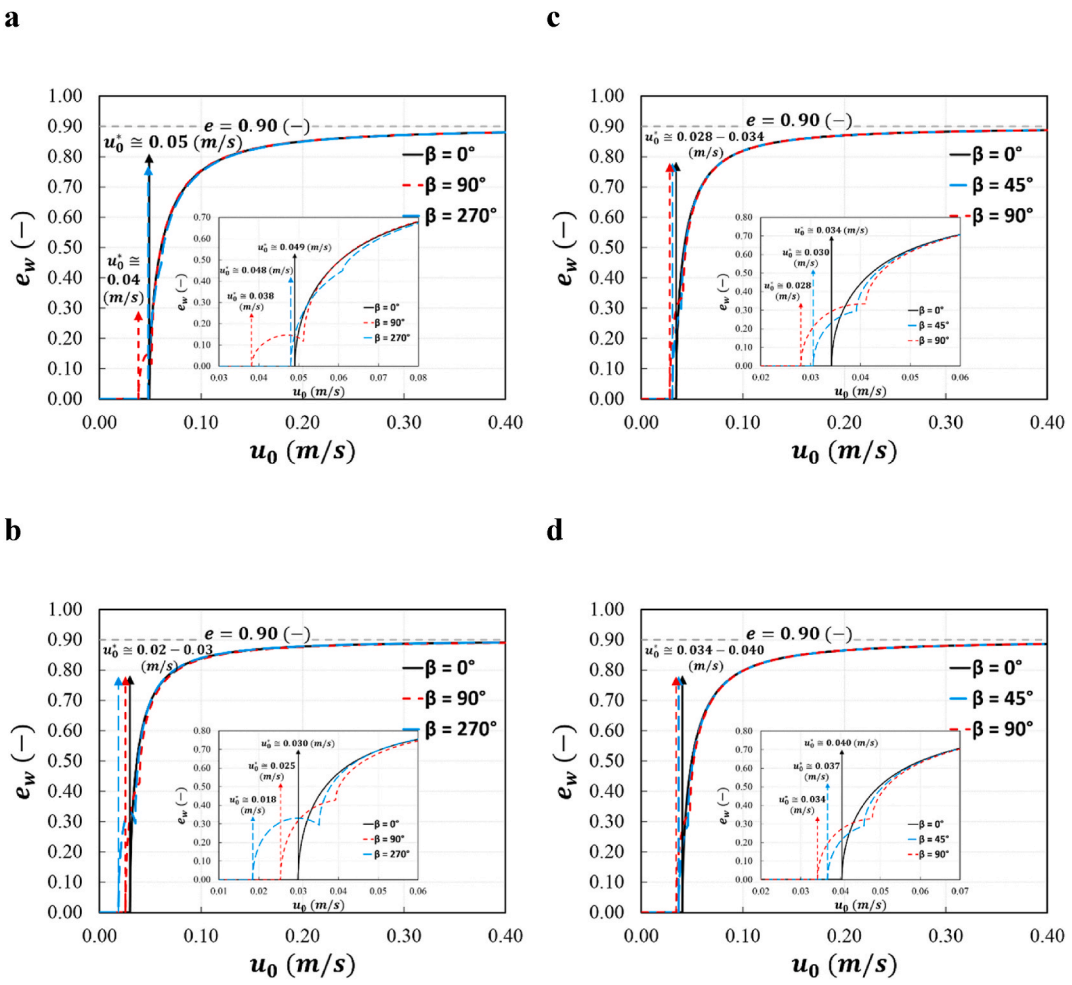

Fig. 8. Effects of collision angle and a) solid particle diameter, b) solid particle density, c) surface asperity heights and d) thickness of liquid coating layers on the outcome of a binary collision of particles coated with water. Reference case conditions are listed in Table 2, while varied parameters are listed in Table 3.

heights causes the colliding particles to travel longer distances during the approach and separation stages, thus resulting in greater energy losses. This result highlights that a proper measurement of the surface asperity size has a critical role for the prediction of collision outcomes under viscous limiting conditions. LaMarche et al. [63] has recently introduced a measurement method to quantify surface roughness for accurate cohesive force predictions.

The effects of distribution and sum of the thickness of liquid coatings on the collision outcomes were investigated next. We first changed the distribution of coating thicknesses, while keeping their sum constant. As a result, only negligible changes, which can hardly be distinguished in the presented results, due to slight changes in mass of colliding particles, were obtained in e_w vs. u_0 profiles of water and slag coatings (compare Figs. 6b and S.2b and Figs. 6d and S.3b for the water and slag cases, respectively). Nonetheless, simultaneous increase of $h_{0,i}$ and $h_{0,j}$, according to the values reported in Table 3 for cases with water and slag coatings, increase u_0^* for all collision angles (Fig. 6b vs. Fig. 8d for water and Fig. 6d vs. Fig. 9d for slag). This observation is in a broad agreement with results presented in Shabanian et al. [31]. The effect is significantly more pronounced with slag. The greater losses of kinetic energy that take place for an extended particle collision distance with thicker coatings explains this observation. It is worth highlighting that we reach the same conclusion as what was achieved by results presented in Figs. 6b and d for the effect of collision angle on the collision outcomes when scrutinizing Figs. 8 and 9, S-2 and S-3.

3.4. Monte Carlo uncertainty analyses

This section of the study aims at investigating the variability in e_w in the presence of uncertainty in some important input parameters of the generalized agglomeration model. We adopted Monte Carlo sampling as the uncertainty propagation method. According to this method, a large number of sample points are randomly selected from the distribution of uncertain parameters and fed into a primary model to propagate uncertainty and, hence, quantify output variability, which is typically represented as a probability

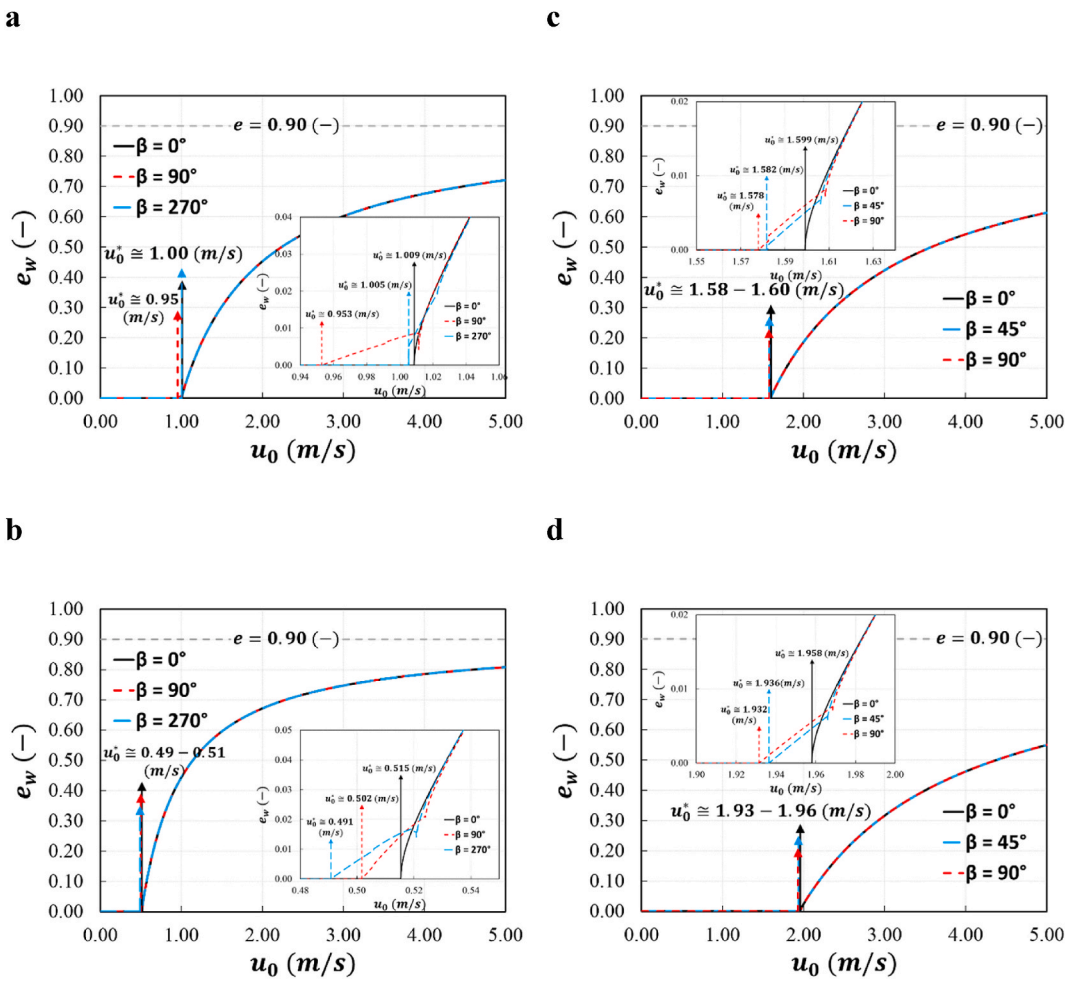

Fig. 9. Effects of collision angle and a) solid particle diameter, b) solid particle density, c) surface asperity heights and d) thickness of liquid coating layers on the outcome of a binary collision of particles coated with slag. Reference case conditions are listed in Table 2, while varied parameters are listed in Table 3.

Table 4
Mean and standard deviations of uncertain parameters for two sets of Monte Carlo uncertainty analyses.

Uncertain parameters	Case I: water			Case II: hypothetical slag		
	mean	*reference standard deviation*	*alternative standard deviations*	*mean*	*reference standard deviation*	*alternative standard deviations*
$d_{p,s,i}$ (μm)	1000	10	3.33, 33.33	1000	10	3.33, 33.33
$d_{p,s,j}$ (μm)	1000	10	3.33, 33.33	1000	10	3.33, 33.33
$h_{a,i}$ (μm)	0.10	0.005	0.0025, 0.010	0.10	0.005	0.0025, 0.010
$h_{a,j}$ (μm)	0.10	0.005	0.0025, 0.010	0.10	0.005	0.0025, 0.010
$h_{0,i}$ (μm)	5.00	0.10	0.05, 0.15	0.15	0.01	0.005, 0.015
$h_{0,j}$ (μm)	5.00	0.10	0.05, 0.15	0.15	0.01	0.005, 0.015
μ_l (Pa.s)	8.9×10^{-4}	7.42×10^{-5} (25% error)	2.97×10^{-5} (10% error), 1.48×10^{-4} (50% error)	10.0	0.833 (25% error)	0.333 (10% error), 1.670 (50% error)
γ_l (N/m)	0.073	0.00608 (25% error)	0.00243 (10% error)	0.400	0.033 (25% error)	0.0133 (10% error)
u_0 (m/s)	0.0425	0.00425 (30% error)	0.00142 (10% error), 0.00708 (50% error)	1.50	0.15 (30% error)	0.05 (10% error), 0.25 (50% error)
	0.0347	0.00347 (30% error)	0.00116 (10% error), 0.00578 (50% error)	0.81	0.081 (30% error)	0.027 (10% error), 0.135 (50% error)

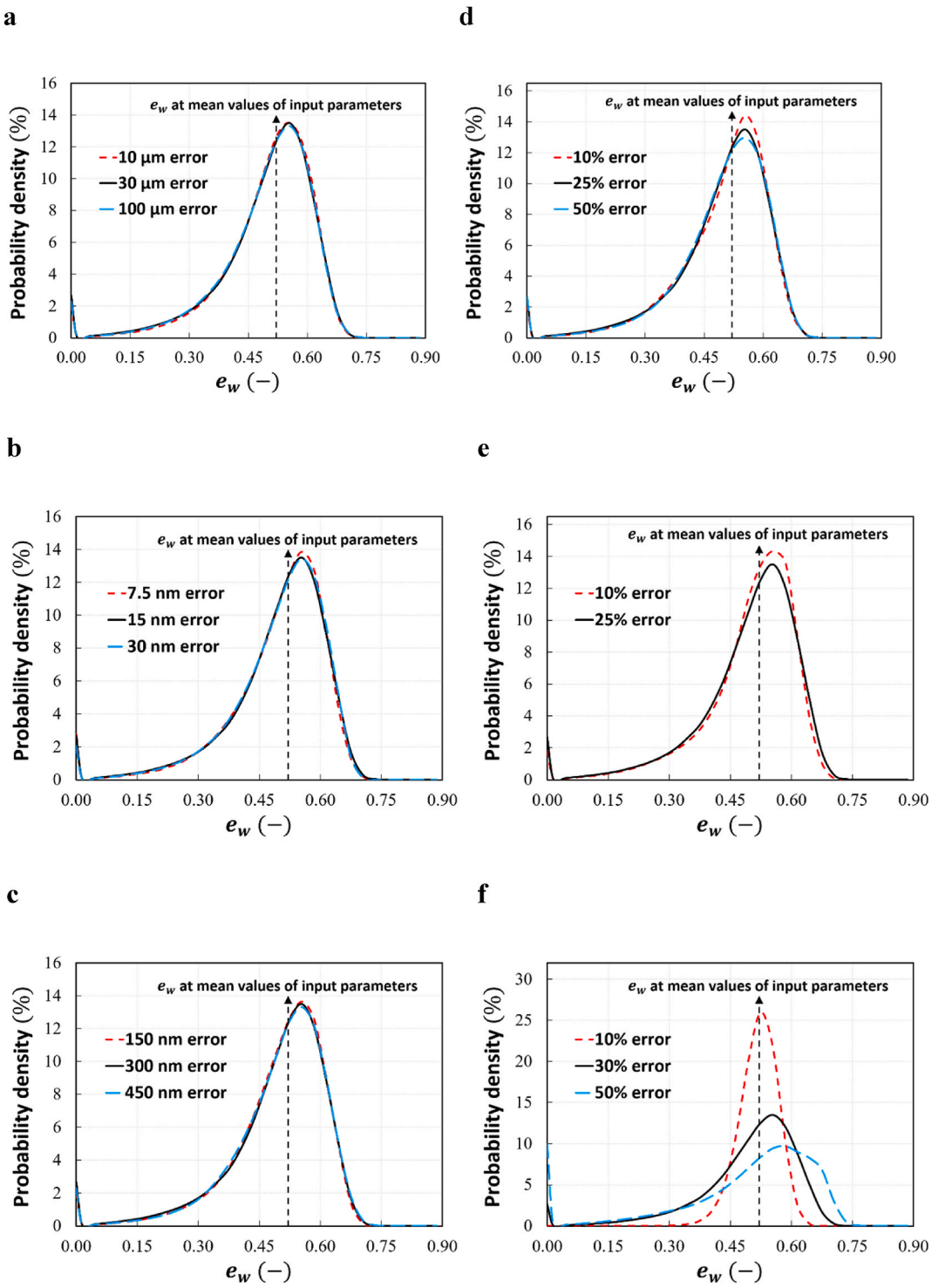

Fig. 10. Probability density of e_w when changing uncertainties of a) solid particle diameters, b) surface asperity heights, c) thickness of liquid coating layers, d) liquid viscosity, e) surface tension, and f) u_0 for a binary collision of wet particles coated with water; $e_w \cong 0.52$ with mean values of input parameters. Conditions are presented in Table 4.

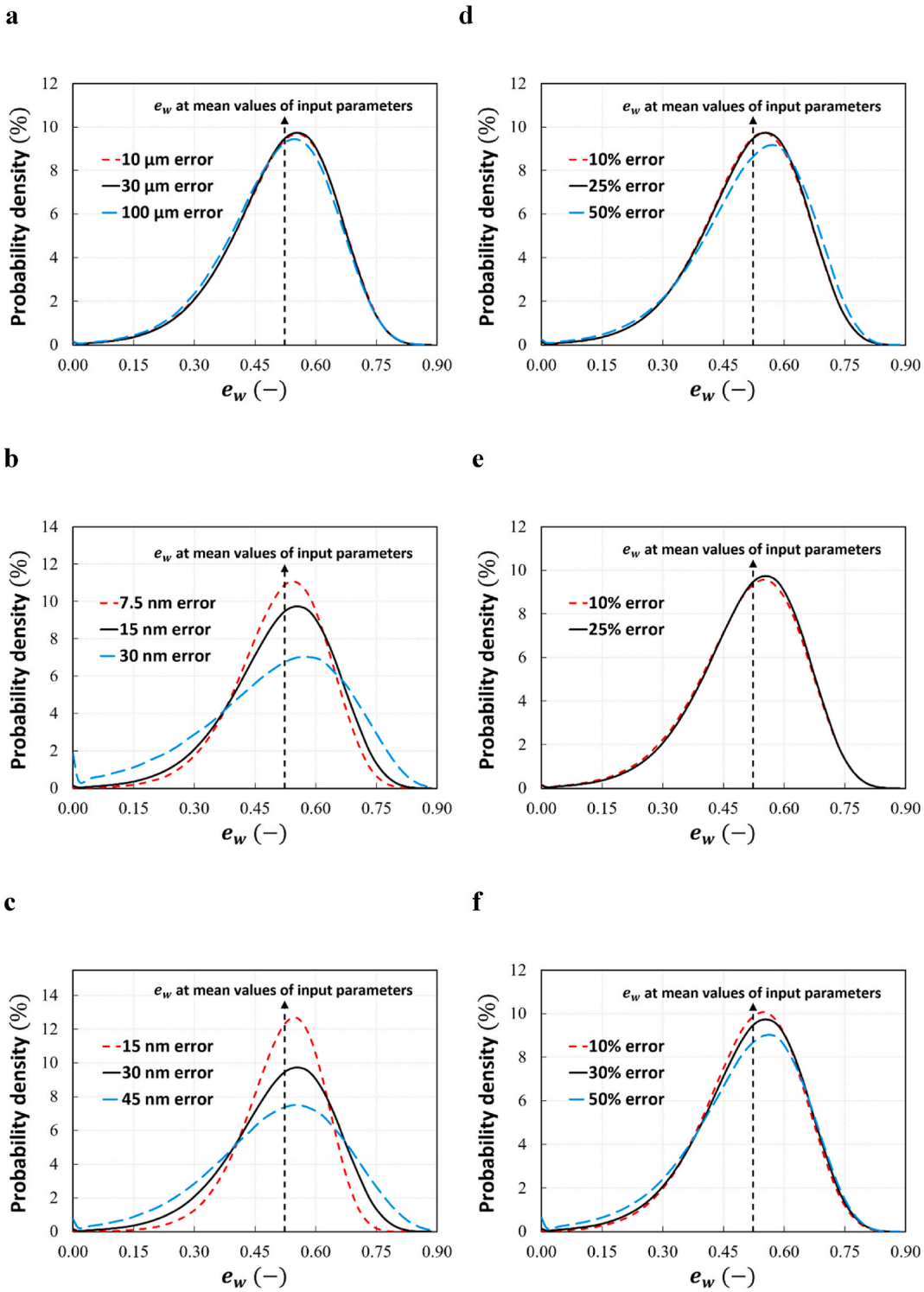

Fig. 11. Probability density of e_w when changing uncertainties of a) solid particle diameters, b) surface asperity heights, c) thickness of liquid coating layers, d) liquid viscosity, e) surface tension, and f) u_0 for a binary collision of wet particles coated with slag; $e_w \cong 0.52$ with mean values of input parameters. Conditions are presented in Table 4.

density function [64–66]. In the present study, we employed the generalized agglomeration model as the primary model, with e_w being the output variable, and considered normal distributions in the uncertain parameters. The mean values of nearly all input parameters are the same as the reference cases described in Table 2. For the first input set, we selected a mean u_0 such that the e_w with the mean input parameters is about 0.52 for both water and slag cases. In the second set, the mean u_0 was adjusted to yield $e_w \cong 0.20$ for both cases when employing mean values of input parameters. While we discuss the results with the first set in this section, the results with the second set, which are in broad agreement with those of the first, are presented in Section S-14 of the Supplementary Material. The mean and standard deviations of uncertain parameters selected here are reported in Table 4. For each uncertain parameter, a reference and one or two alternative standard deviations, inspired by practical applications, were considered. When performing the uncertainly analysis employing an alternative standard deviation for an uncertain parameter, the reference values for standard deviations of other uncertain parameters were applied. The results of each uncertainty analysis presented in this study are based on 1,000,000 Monte Carlo samples that were randomly generated for uncertain parameters. Varying the number of Monte Carlo samples between 500,000 and 5,000,000 had a minimal influence on the probability density of e_w for both water and slag reference cases (Fig. S.4). Hence, we conducted the analyses based on 1,000,000 samples to balance the accuracy in the output probability density and computational expenses.

The results of uncertainty analyses for water and slag coatings, when e_w at mean values of input parameters for these cases was about 0.52, are presented in Figs. 10 and 11, respectively. For all uncertainty analysis scenarios studied here, e_w shows a distribution around its mean that can span in the range of $0 \leq e_w < e$. This observation indicates that if a system of wet particles operates near u_0^*, an uncertainty analysis is required to provide a more comprehensive evaluation of the agglomeration tendency of the system. The results presented in Fig. 10 reveal that, under capillary limiting conditions, (i) uncertainties in the solid particle size, asperity heights, and thickness of liquid coating layers have negligible effects on the variability of e_w, (ii) the probability density of e_w slightly varies around its mean owing to uncertainties in the liquid viscosity and surface tension, and (iii) the uncertainty in u_0 has the greatest influence on the variability of e_w. Therefore, among various uncertain parameters that can affect the variability of e_w, an accurate estimation of u_0 is crucial for the reliable prediction of collision outcomes under capillary limiting conditions and at impact speeds near u_0^*. We can reach the same conclusion by analyzing the results presented in Fig. S.5 when $e_w \cong 0.20$ with mean values of input parameters for particles coated with water.

According to the results presented in Fig. 11, under viscous limiting conditions, (i) uncertainties in the surface tension and solid particle size have relatively negligible effects on the variability of e_w, (ii) the liquid viscosity and u_0 can slightly change the probability density of e_w, and (iii) the probability density of e_w is significantly influenced by uncertainties in asperity heights and thickness of liquid coating layers. Similar observations, which are less pronounced than those observed in Fig. 11, can be obtained by analyzing Fig. S.6 when $e_w \cong 0.20$ with mean values of input parameters for particles coated with slag. The considerable effects of uncertainties in asperity heights and thickness of liquid coating layers in the variability of e_w can be attributed to the substantial roles of these parameters in the magnitude of the viscous force and the resulting loss of kinetic energy, which governs the collision outcome under viscous limiting conditions. These observations suggest that for the realistic prediction of collision outcomes under viscous limiting conditions, we need to accurately measure/estimate asperity heights and thickness of liquid coating layers. For example, if alkali material from fuel ash in a fluidized bed combustor reacts with bed particles to form a viscous coating, the accuracy of thermodynamic calculations to estimate the amount of produced liquid and, hence, the thickness of the coating, may be critical in the prediction of collision outcomes.

4. Conclusion

This work presents a generalized analytical energy balance model for evaluating agglomeration from binary collisions of wet particles. The model simultaneously considers the effects of body forces, solid-solid contacting, and liquid bridge volume-corrected capillary and viscous forces. Hence, it can handle collisions of wet particles differing in particle properties, coating thicknesses, and impact speeds. We verified the model by comparing its predictions with those from the non-generalized analytical energy balance model [31] for binary collisions of identical wet particles under both capillary and viscous limiting conditions. We validated the model by comparing its predictions with experimental data from Buck et al. [12]. Investigating the effect of collision direction on the outcome of a binary collision of wet particles indicated that it can only influence the collision outcome and/or value of e_w at impact speeds close to the critical impact speed, where the magnitude of net body forces along the collision axis approaches the magnitudes of governing interparticle forces. The effect is relatively negligible if impact speeds of colliding wet particles deviate sufficiently from the critical impact speed. Analyzing the results of Monte Carlo uncertainty analyses with the generalized agglomeration model indicated that for the realistic prediction of collision outcomes, we need to accurately measure/estimate the impact speed, under capillary limiting conditions, and thickness of coating layers and asperity heights, under viscous limiting conditions. The proposed model can be incorporated with a mathematical basis that monitors particle agglomerates, which can proceed with growth or breakage in a processing unit, i.e., in detailed computational fluid dynamics codes that track particle collisions. It can, hence, help describe the complex particle-particle interactions that occur during the processing of wet particles and clarify the mechanism of particle agglomeration.

Nomenclature

See Section S-1 of the Supplementary Material.

CRediT authorship contribution statement

Jaber Shabanian: Conceptualization, Methodology, Software, Validation, Formal analysis, Investigation, Data curation, Writing – Original draft preparation, Visualization. **Marc A. Duchesne:** Conceptualization, Investigation, Writing – Reviewing and Editing. **Madhava Syamlal:** Conceptualization, Writing – Reviewing and Editing. **Allan Runstedtler:** Resources, Writing – Reviewing and Editing, Supervision, Project administration, Funding acquisition.

Declaration of competing interest

The authors declare that they have no known competing financial interests or personal relationships that could have appeared to influence the work reported in this paper.

Acknowledgements

This work was supported by the Government of Canada's Program of Energy Research and Development (Project code: CEO-19-114). The authors are grateful to Dr. Robin Hughes for valuable discussions.

Supplementary Material

Supplementary material to this article can be found online at https://doi.org/10.1016/j.heliyon.2024.e26320.

References

[1] M. Bartels, W. Lin, J. Nijenhuis, F. Kapteijn, J.R. van Ommen, Agglomeration in fluidized beds at high temperatures: mechanisms, detection and prevention, Prog. Energy Combust. Sci. 34 (2008) 633–666, https://doi.org/10.1016/j.pecs.2008.04.002.
[2] P. Darabi, K. Pougatch, M. Salcudean, D. Grecov, A novel coalescence model for binary collision of identical wet particles, Chem. Eng. Sci. 64 (2009) 1868–1876, https://doi.org/10.1016/j.ces.2009.01.017.
[3] Y. Zhou, Q. Shi, Z. Huang, J. Wang, Y. Yang, Particle agglomeration and control of gas-solid fluidized bed reactor with liquid bridge and solid bridge coupling actions, Chem. Eng. J. 330 (2017) 840–851, https://doi.org/10.1016/j.cej.2017.07.117.
[4] C.M. Boyce, Gas-solid fluidization with liquid bridging: a review from a modeling perspective, Powder Technol. 336 (2018) 12–29, https://doi.org/10.1016/j.powtec.2018.05.027.
[5] J.D. Morris, S.S. Daood, S. Chilton, W. Nimmo, Mechanisms and mitigation of agglomeration during fluidized bed combustion of biomass: a review, Fuel 230 (2018) 452–473, https://doi.org/10.1016/j.fuel.2018.04.098.
[6] S.J.R. Simons, J.P.K. Seville, M.J. Adams, An analysis of the rupture energy of pendular liquid bridges, Chem. Eng. Sci. 49 (1994) 2331–2339, https://doi.org/10.1016/0009-2509(94)E0050-Z.
[7] J.R. van Ommen, M.-O. Coppens, C.M. van den Bleek, J.C. Schouten, Early warning of agglomeration in fluidized beds by attractor comparison, AIChE J. 46 (2000) 2183–2197, https://doi.org/10.1002/aic.690461111.
[8] L.A. Noble, Method of Preventing or Reducing Polymer Agglomeration on Grid in Fluidized-Bed Reactors, 2012. Patent US8129482 B2, https://patentscope.wipo.int/search/en/detail.jsf?docId=WO2009108434&tab=PCTBIBLIO&maxRec=1000.
[9] B. Crüger, S. Heinrich, S. Antonyuk, N.G. Deen, J.A.M. Kuipers, Experimental study of oblique impact of particles on wet surfaces, Chem. Eng. Res. Des. 110 (2016) 209–219, https://doi.org/10.1016/j.cherd.2016.01.024.
[10] B. Crüger, V. Salikov, S. Heinrich, S. Antonyuk, V.S. Sutkar, N.G. Deen, J.A.M. Kuipers, Coefficient of restitution for particles impacting on wet surfaces: an improved experimental approach, Particuology 25 (2016) 1–9, https://doi.org/10.1016/j.partic.2015.04.002.
[11] B. Buck, Y. Tang, S. Heinrich, N.G. Deen, J.A.M. Kuipers, Collision dynamics of wet solids: rebound and rotation, Powder Technol. 316 (2017) 218–224, https://doi.org/10.1016/j.powtec.2016.12.088.
[12] B. Buck, J. Lunewski, L. Tang, N.G. Deen, J.A.M. Kuipers, S. Heinrich, Numerical investigation of collision dynamics of wet particles via force balance, Chem. Eng. Res. Des. 132 (2018) 1143–1159, https://doi.org/10.1016/j.cherd.2018.02.026.
[13] P. Grohn, T. Oesau, S. Heinrich, S. Antonyuk, Investigation of the influence of impact velocity and liquid bridge volume on the maximum liquid bridge length, Adv. Powder Technol. 33 (2022) 103630 (12 pages). 10.1016/j.apt.2022.103630.
[14] R.J. Fairbrother, S.J.R. Simons, Modelling of binder-induced agglomeration, Part. Part. Syst. Char. 15 (1998) 16–20, https://doi.org/10.1002/(SICI)1521-4117(199802)15:1<16::AID-PPSC16>3.0.CO;2-1.
[15] C.D. Willett, J.P.K. Seville, An examination of the effects of contact angle on the properties of exact and toroidal liquid bridges, in: Proceedings of the 3rd World Congress on Particle Technology, The Brighton Centre, UK, 1998. Paper 79.
[16] S.J.R. Simons, R.J. Fairbrother, Direct observations of liquid binder–particle interactions: the role of wetting behaviour in agglomerate growth, Powder Technol. 110 (2000) 44–58, https://doi.org/10.1016/S0032-5910(99)00267-3.
[17] D. Rossetti, X. Pepin, S.J.R. Simons, Rupture energy and wetting behavior of pendular liquid bridges in relation to the spherical agglomeration process, J. Colloid Interface Sci. 261 (2003) 161–169, https://doi.org/10.1016/S0021-9797(03)00043-2.
[18] R.H. Davis, J.-M. Serayssol, E.J. Hinch, The elastohydrodynamic collision of two spheres, J. Fluid Mech. 163 (1986) 479–497, https://doi.org/10.1017/S0022112086002392.
[19] G. Barnocky, R.H. Davis, Elastohydrodynamic collision and rebound of spheres: experimental verification, Phys. Fluids 31 (1988) 1324–1329, https://doi.org/10.1063/1.866725.
[20] B.J. Ennis, J. Li, G.I. Tardos, R. Pfeffer, The influence of viscosity on the strength of an axially strained pendular liquid bridge, Chem. Eng. Sci. 45 (1990) 3071–3088, https://doi.org/10.1016/0009-2509(90)80054-I.
[21] A.A. Adetayo, J.D. Litster, S.E. Pratsinis, B.J. Ennis, Population balance modelling of drum granulation of materials with wide size distribution, Powder Technol. 82 (1995) 37–49, https://doi.org/10.1016/0032-5910(94)02896-V.

[22] J.D. Litster, R. Sarwono, Fluidized drum granulation: studies of agglomerate formation, Powder Technol. 88 (1996) 165–172, https://doi.org/10.1016/0032-5910(96)03116-6.
[23] G.G. Joseph, R. Zenit, M.L. Hunt, A.M. Rosenwinkel, Particle–wall collisions in a viscous fluid, J. Fluid Mech. 433 (2001) 329–346, https://doi.org/10.1017/S0022112001003470.
[24] R.H. Davis, D.A. Rager, B.T. Good, Elastohydrodynamic rebound of spheres from coated surfaces, J. Fluid Mech. 468 (2002) 107–119, https://doi.org/10.1017/S0022112002001489.
[25] A. Braumann, M.J. Goodson, M. Kraft, P.R. Mort, Modelling and validation of granulation with heterogeneous binder dispersion and chemical reaction, Chem. Eng. Sci. 62 (2007) 4717–4728, https://doi.org/10.1016/j.ces.2007.05.028.
[26] T. Müller, K. Huang, Influence of the liquid film thickness on the coefficient of restitution for wet particles, Phys. Rev. E 93 (2016) 042904. https://link.aps.org/doi/10.1103/PhysRevE.93.042904.
[27] S. Antonyuk, S. Heinrich, N. Deen, H. Kuipers, Influence of liquid layers on energy absorption during particle impact, Particuology 7 (2009) 245–259, https://doi.org/10.1016/j.partic.2009.04.006.
[28] F. Gollwitzer, I. Rehberg, C.A. Kruelle, K. Huang, Coefficient of restitution for wet particles, Phys. Rev. E 86 (2012) 011303. https://link.aps.org/doi/10.1103/PhysRevE.86.011303.
[29] B.V. Balakin, S. Alyaev, A.C. Hoffmann, P. Kosinski, Micromechanics of agglomeration forced by the capillary bridge: the restitution of momentum, AIChE J. 59 (2013) 4045–4057, https://doi.org/10.1002/aic.14162.
[30] V.S. Sutkar, N.G. Deen, J.T. Padding, J.A.M. Kuipers, V. Salikov, B. Crüger, S. Antonyuk, S. Heinrich, A novel approach to determine wet restitution coefficients through a unified correlation and energy analysis, AIChE J. 61 (2015) 769–779, https://doi.org/10.1002/aic.14693.
[31] J. Shabanian, M.A. Duchesne, A. Runstedtler, M. Syamlal, R.W. Hughes, Improved analytical energy balance model for evaluating agglomeration from a binary collision of identical wet particles, Chem. Eng. Sci. 223 (2020) 115738, https://doi.org/10.1016/j.ces.2020.115738.
[32] L. Hua, R. Ocone, N. Yang, CFD-DEM simulations of wet particles fluidization with a new evolution model for liquid bridge, 2022, AIChE J. 68 (2022) e17681 (15 pages). 10.1002/aic.17681.
[33] M. Rydén, M. Hanning, A. Corcoran, F. Lind, Oxygen Carrier Aided Combustion (OCAC) of wood chips in a semi-commercial circulating fluidized bed boiler using manganese ore as bed material, Appl. Sci. 6 (2016) 347 (19 pages). 10.3390/app6110347.
[34] R.W. Hughes, D.Y. Lu, R.T. Symonds, Improvement of oxy-FBC using oxygen carriers: concept and combustion performance, Energy Fuels 31 (2017) 10101–10115, https://doi.org/10.1021/acs.energyfuels.7b01556.
[35] M.J. Matthewson, Adhesion of spheres by thin liquid films, Philos. Mag. A 57 (1988) 207–216, https://doi.org/10.1080/01418618808204510.
[36] O. Pitois, P. Moucheront, X. Château, Rupture energy of a pendular liquid bridge, Eur. Phys. J. B 23 (2001) 79–86, https://doi.org/10.1007/s100510170084.
[37] H.R. Norouzi, R. Zarghami, R. Sotudeh Gharebaagh, N. Mostoufi, Coupled CFD-DEM Modeling: Formulation, Implementation and Application to Multiphase Flows, John Wiley & Sons, Chitester, UK, 2016.
[38] B. Derjaguin, Untersuchungen über die Reibung und Adhäsion, IV, Kolloid Z. 69 (1934) 155–164, https://doi.org/10.1007/BF01433225.
[39] J.N. Israelachvili, Intermolecular and Surface Forces, Academic Press, Amsterdam, 2003.
[40] O. Pitois, P. Moucheront, X. Château, Liquid bridge between two moving spheres: an experimental study of viscosity effects, J. Colloid Interface Sci. 231 (2000) 26–31, https://doi.org/10.1006/jcis.2000.7096.
[41] V.A. Lubarda, K.A. Talke, Analysis of the equilibrium droplet shape based on an ellipsoidal droplet model, Langmuir 2 (2011) 10705–10713, https://doi.org/10.1021/la202077w.
[42] J. Shabanian, J. Chaouki, Effects of temperature, pressure, and interparticle forces on the hydrodynamics of a gas-solid fluidized bed, Chem. Eng. J. 313 (2017) 580–590, https://doi.org/10.1016/j.cej.2016.12.061.
[43] S. Hamzehlouia, J. Shabanian, M. Latifi, J. Chaouki, Effect of microwave heating on the performance of catalytic oxidation of n-butane in a gas-solid fluidized bed reactor, Chem. Eng. Sci. 192 (2018) 1177–1188, https://doi.org/10.1016/j.ces.2018.08.054.
[44] J. Chaouki, S. Farag, M. Attia, J. Doucet, The development of industrial (thermal) processes in the context of sustainability: the case for microwave heating, Can. J. Chem. Eng. 98 (2020) 832–847, https://doi.org/10.1002/cjce.23710.
[45] K. Adavi, A. Amini, M. Latifi, J. Shabanian, J. Chaouki, Kinetic study of multiphase reactions under microwave irradiation: a mini-review, Front. Chem. Eng. 4 (2022) 1059160 (8 pages). 10.3389/fceng.2022.105916.
[46] H.D. Young, R.A. Freedman, Sears and Zemansky's University Physics with Modern Physics, Addison Wesley, Boston, MA, US, 2012.
[47] D. Gidaspow, Multiphase Flow and Fluidization: Continuum and Kinetic Theory Descriptions, Academic Press, Boston, MA, US, 1994.
[48] C.D. Willett, M.J. Adams, S.A. Johnson, J.P.K. Seville, Capillary bridges between two spherical bodies, Langmuir 16 (2000) 9396–9405, https://doi.org/10.1021/la000657y.
[49] F.P. Di Maio, A. Di Renzo, Capillary interaction for DEM simulations of wet particulate materials, in: 8th World Congress on Particle Technology, 2018 (Orlando, Florida, US).
[50] J.M. Link, W. Godlieb, P. Tripp, N.G. Deen, S. Heinrich, J.A.M. Kuipers, M. Schönherr, M. Peglow, Comparison of fibre optical measurements and discrete element simulations for the study of granulation in a spout fluidized bed, Powder Technol. 189 (2009) 202–217, https://doi.org/10.1016/j.powtec.2008.04.017.
[51] B. Gatternig, J. Karl, Application of chemical equilibrium calculations for the prediction of ash-induced agglomeration, Biomass Convers. Biorefin. 9 (2019) 117–128, https://doi.org/10.1007/s13399-018-0325-7.
[52] P.N. Rowe, L. Santoro, J.G. Yates, The division of gas between bubble and interstitial phases in fluidised beds of fine powders, Chem. Eng. Sci. 33 (1978) 133–140, https://doi.org/10.1016/0009-2509(78)85079-9.
[53] J.G. Yates, D. Newton, Fine particle effects in a fluidized-bed reactor, Chem. Eng. Sci. 41 (1986) 801–806, https://doi.org/10.1016/0009-2509(86)87160-3.
[54] H. Cui, N. Mostoufi, J. Chaouki, Characterization of dynamic gas-solid distribution in fluidized beds, Chem. Eng. J. 79 (2000) 133–143, https://doi.org/10.1016/S1385-8947(00)00178-9.
[55] H. Cui, N. Mostoufi, J. Chaouki, Gas and solids between dynamic bubble and emulsion in gas-fluidized beds, Powder Technol. 120 (2001) 12–20, https://doi.org/10.1016/S0032-5910(01)00341-2.
[56] J. Shabanian, J. Chaouki, Local characterization of a gas-solid fluidized bed in the presence of thermally induced interparticle forces, Chem. Eng. Sci. 119 (2014) 261–273, https://doi.org/10.1016/j.ces.2014.08.037.
[57] C.Y. Wen, Y.H. Yu, A generalized method for predicting the minimum fluidization velocity, AIChE J. 12 (1966) 610–612, https://doi.org/10.1002/aic.690120343.
[58] H. Do, A. Aragon, D. Schott, Automated discrete element method calibration using genetic and optimization algorithms, in: Proceedings of the 8th International Conference on Micromechanics on Granular Media: Powders and Grains, EDP Sciences, Les Ulis Cedex A, France, 2017.
[59] B.J. Ennis, G. Tardos, R. Pfeffer, A microlevel-based characterization of granulation phenomena, Powder Technol. 65 (1991) 257–272, https://doi.org/10.1016/0032-5910(91)80189-.
[60] Y. Zhong, J. Gao, Z. Wang, Z. Guo, Influence of particle size distribution on agglomeration/defluidization of iron powders at elevated temperature, ISIJ Int. 57 (2017) 1–7, https://doi.org/10.2355/isijinternational.ISIJINT-2016-487.
[61] A. Corcoran, J. Marinkovic, F. Lind, H. Thunman, P. Knutsson, M. Seemann, Ash properties of ilmenite used as bed material for combustion of biomass in a circulating fluidized bed boiler, Energy Fuels 28 (2014) 7672–7679, https://doi.org/10.1021/ef501810u.
[62] E. Garcia, H. Liu, Ilmenite as alternative bed material for the combustion of coal and biomass blends in a fluidized bed combustor to improve combustion performance and reduce agglomeration tendency, Energy 239 (2022) 121913 (14 pages). 10.1016/j.energy.2021.121913.
[63] C.Q. LaMarche, S. Leadley, P. Liu, K.M. Kellogg, C.M. Hrenya, Method of quantifying surface roughness for accurate adhesive force predictions, Chem. Eng. Sci. 158 (2017) 140–153, https://doi.org/10.1016/j.ces.2016.09.024.

[64] M.J.W. Jansen, W.A.H. Rossing, R.A. Daamen, Monte Carlo estimation of uncertainty contributions from several independent multivariate sources, in: J. Grasman, G. van Straten (Eds.), Predictability and Nonlinear Modelling in Natural Sciences and Economics, Springer, Dordrecht, 1994, https://doi.org/10.1007/978-94-011-0962-8_28.

[65] M.H. Sahraei, M.A. Duchesne, R.W. Hughes, L.A. Ricardez-Sandoval, Experimental assessment, model validation, and uncertainty quantification of a pilot-scale gasifier, Ind. Eng. Chem. Res. 55 (2016) 6961–6970, https://doi.org/10.1021/acs.iecr.6b00692.

[66] L.L. Simon, M. Dieckmann, A. Robinson, T. Vent-Schmidt, D. Marantelli, R. Kohlbrenner, A. Saint-Dizier, D. Gribkov, J.-P. Krieger, Monte Carlo analysis-based CapEx uncertainty estimation of new technologies: the case of photochemical lamps, Org. Process Res. Dev. (2021), https://doi.org/10.1021/acs.oprd.1c00245.